MICROCOPY RESOLUTION TEST CHART
NATIONAL BUREAU OF STANDARDS-1963-A

AIR FORCE ACADEMY
Aeronautics Digest

DTIC
ELECTED
S MAR 0 4 1986 **D**
D
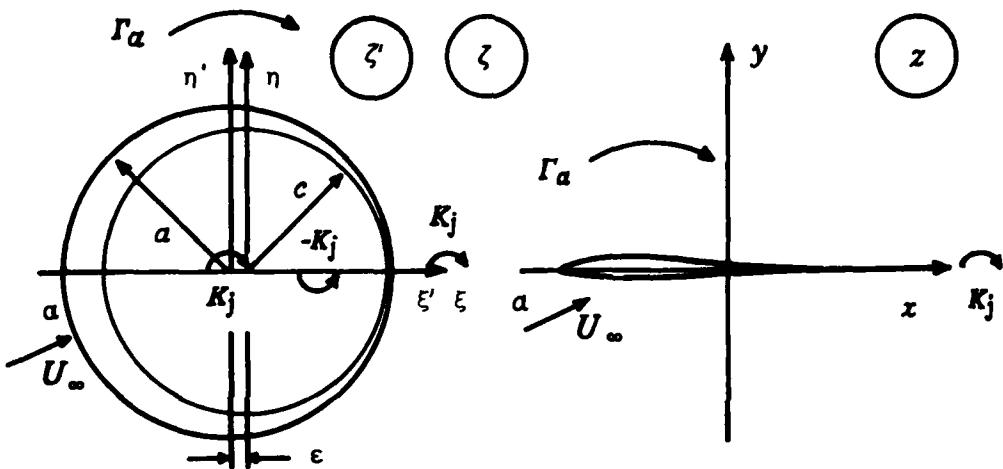
SEPTEMBER 1985
Final Report

APPROVED FOR PUBLIC RELEASE: DISTRIBUTION UNLIMITED

06 3

COVER:
The cover shows both the physical and computational planes for a circular cylinder undergoing a Joukowski transformation. This classic analytical method was applied by Major John Russell and Professor Chuen-Yen Chow to study the unsteady lift generated by a flat plate airfoil undergoing time dependent chord deformations. For details of the analysis, readers are directed to Major Russell's and Professor Chow's article, which is presented in this issue of the Aeronautics Digest.

Editorial Review by Capt. Michael Hale, Department of English, USAF Academy, Colorado Springs, Colorado 80840.

THOMAS E. McCANN, Lt Col, USAF
Director of Research and
Computer Based Education

ADA 164941

REPORT DOCUMENTATION PAGE

1a. REPORT SECURITY CLASSIFICATION UNCLASSIFIED	1b. RESTRICTIVE MARKINGS
2a. SECURITY CLASSIFICATION AUTHORITY	3. DISTRIBUTION/AVAILABILITY OF REPORT Approved for public release. Distribution unlimited.
2b. DECLASSIFICATION/DOWNGRADING SCHEDULE	
4. PERFORMING ORGANIZATION REPORT NUMBER(S) USAFA-TR-85-11	5. MONITORING ORGANIZATION REPORT NUMBER(S)

6a. NAME OF PERFORMING ORGANIZATION	6b. OFFICE SYMBOL (If applicable)	7a. NAME OF MONITORING ORGANIZATION
Department of Aeronautics		
6c. ADDRESS (City, State and ZIP Code) U.S. Air Force Academy Colorado Springs, CO 80840-5831		7b. ADDRESS (City, State and ZIP Code)

8a. NAME OF FUNDING/SPONSORING ORGANIZATION	8b. OFFICE SYMBOL (If applicable)	9. PROCUREMENT INSTRUMENT IDENTIFICATION NUMBER

8c. ADDRESS (City, State and ZIP Code)	10. SOURCE OF FUNDING NOS.			
	PROGRAM ELEMENT NO.	PROJECT NO.	TASK NO.	WORK UNIT NO.

11. TITLE (Include Security Classification)
Air Force Academy Aeronautics Digest

12. PERSONAL AUTHOR(S)
Editors: Russell, J., Hale, M.

13a. TYPE OF REPORT Final Report	13b. TIME COVERED FROM _____ TO _____	14. DATE OF REPORT (Yr., Mo., Day) September 1985	15. PAGE COUNT

16. SUPPLEMENTARY NOTATION

17. COSATI CODES			18. SUBJECT TERMS (Continue on reverse if necessary and identify by block number)
FIELD	GROUP	SUB. GR.	Unsteady aerodynamics; vortex wake; dynamic stall; pressure measurements; data reduction; airbreathing propulsion; propulsion curriculum; examination scores.

19. ABSTRACT (Continue on reverse if necessary and identify by block number)
This Digest covers unclassified research in aeronautics performed by individuals assigned to or associated with the United States Air Force Academy. This report includes technical papers in the specific areas of aerodynamics and engineering education.

20. DISTRIBUTION/AVAILABILITY OF ABSTRACT UNCLASSIFIED/UNLIMITED ☒ SAME AS RPT ☐ DTIC USERS ☐	21. ABSTRACT SECURITY CLASSIFICATION UNCLASSIFIED	
22a. NAME OF RESPONSIBLE INDIVIDUAL Major John H. Russell	22b. TELEPHONE NUMBER (Include Area Code) 303-472-4010	22c. OFFICE SYMBOL DFAN

DD FORM 1473, 83 APR EDITION OF 1 JAN 73 IS OBSOLETE.

PREFACE

This report is the fourteenth issue of the Air Force Academy Aeronautics Digest.* Our policy is to print articles which represent recent scholarly work by students and faculty of the Department of Aeronautics, members of other departments of the Academy and the Frank J. Seiler Research Laboratory, researchers directly or indirectly involved with USAFA-sponsored projects, and authors in fields of interest to the USAFA.

In addition to complete papers, the Digest includes, when appropriate, abstracts of lengthier reports and articles published in other formats. The editors will consider for publication contributions in the general field of Aeronautics, including:

> Aeronautical Engineering
> > Aerodynamics
> > Flight Mechanics
> > Propulsion
> > Structures
> > Instrumentation
> Fluid Dynamics
> Thermodynamics and Heat Transfer
> Biomechanics
> Engineering Education
> Aeronautical History

Papers on other topics will be considered on an individual basis. Contributions should be sent to:

> Editor, Aeronautics Digest
> HQ USAFA/DFAN
> US Air Force Academy
> Colorado Springs, CO 80840-5831

The Aeronautics Digest is edited at present by Maj. John H. Russell, PhD. Capt. Michael Hale provided the final editorial review. Our thanks also to Contract Technical Services, Inc. for illustration services and to Associate Editor, Kathleen S. Brandt.

*Previous issues of the Digest can be ordered from the Defense Technical Information Center (DTIC), Cameron Station, Alexandria, VA 22324.

CONTENTS

Unsteady Forces Acting on a Flat Plate Airfoil Undergoing Chord Deformations

John H. Russell* and Chuen-Yen Chow**

Abstract

This paper investigates the forces generated by a flat plate airfoil that undergoes prescribed chord changes in an otherwise uniform flow. An inviscid and incompressible fluid is assumed and conformal mapping techniques are used to transform a deforming circular cylinder in the computational plane into a flat plate airfoil undergoing chord deformations in the physical plane. The resultant unsteady lift is determined and discussed.

I. Introduction

The utilization of unsteady flow fields for lift enhancement continues to receive the attention of both experimental and theoretical investigators (Ref. 1). A significant number of these studies deal with the generation and control of large vortex structures in the vicinity of the wing upper surface. The large lift increments achieved as a result of these vortex structures have been documented by both experimental (Ref. 2) and theoretical (Ref. 3) efforts. The current study differs from the aforementioned in that unsteady effects enter the problem only through time dependent shape (chord) change undergone by a flat plate airfoil and through the effects of the shed vortex wake. An earlier investigation (Ref. 4) determined that a degree of unsteady lift enhancement arose from prescribed deformations by an elliptical cylinder. That analysis showed this increment to occur in the absence of unsteady circulation about the body and without the associated shed wake. The current study considers the circulatory features of the flow that result from continuous enforcement of the Kutta condition at the trailing edge of a deforming flat plate airfoil, and the effects that these unsteady circulatory features have on the generated lift.

---

*Major, USAF, Instructor, Dept. of Aeronautics, USAF Academy, CO.
**Professor, Dept. of Aerospace Engineering Sciences, Univ. of Colo., Boulder, CO.

II. The Computational Model

In their earlier work, Russell and Chow (Ref. 4) developed a computational model for a circular cylinder deforming radially in a uniform flow that is inclined at an angle of attack α. For the model shown in Figure 1, the complex potential is given by

$$w(\zeta') = U_\infty \left\{ \zeta' e^{-i\alpha} + \frac{a^2}{\zeta'} e^{i\alpha} \right\} + a\, \frac{da}{dt}\, \ln \zeta' \qquad (1)$$
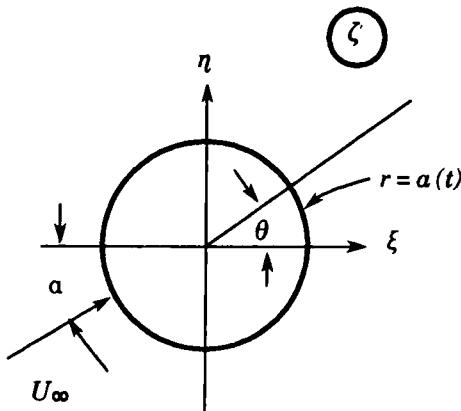
Figure 1. A radially deforming circular cylinder in a
uniform flow at an angle of attack.

Now the model is extended to analyze the unsteady forces arising from prescribed chord deformations of a flat plate airfoil. As a result of continuous enforcement of the Kutta condition, the circulation about the airfoil is itself time dependent. The constancy of circulation, in a global sense, thus requires a shed vortex wake in response to the unsteady bound vortex. The added implications of the unsteady circulation are discussed here and the circulatory terms are added to the previously developed model.

2

Figure 2 depicts the physical airfoil and how, for example, a stretching of the chord results in an unsteady bound vortex and a shed vortex. Circulation of strength Γ_0 is sufficient to insure tangent flow from the trailing edge of the original airfoil whose chord is C_0. Notwithstanding the uncertainties of defining an unsteady Kutta condition in the case of airfoils undergoing oscillatory pitching and vertical translation (Ref. 5), the requirement of flow tangency at the trailing edge will be used throughout this analysis to satisfy the Kutta condition. If, after some time Δt, the chord has grown to C_1, then the previous circulation Γ_0 is insufficient to provide tangent flow from the trailing edge.

Γ_0

C_0

Figure 2a

Γ_0

C_1

Figure 2b

$\Gamma_1 = \Gamma_0 + K$

C_1

$-K$
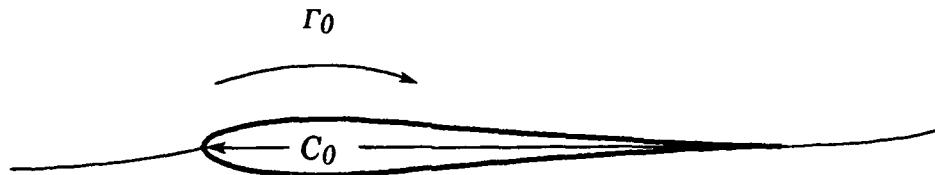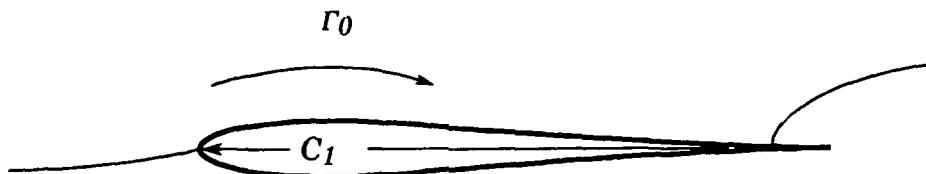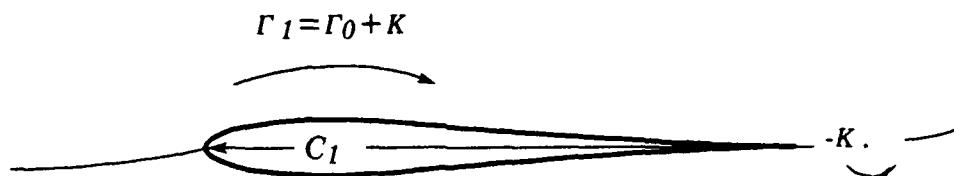
Figure 2c

Figure 2. Enforcement of Kutta condition and constancy of circulation through adjustment of the bound circulation and the shedding of a discrete vortex.

The corresponding flow condition is shown in Fig. 2b where, in fact, an infinite velocity exists at the sharp trailing edge. In order to re-establish tangent flow at the trailing edge, the bound circulation must increase to a value of $\Gamma_1 = \Gamma_0 + K$. In order for the total circulation in the flow to remain constant, vorticity of strength, $-K$, must be shed as shown in Fig. 2c.

In as much as the deformations are continuous in time, so would be the changes in bound vorticity. Likewise, the shed vorticity would be continuously distributed throughout the wake. An analytical solution for this case would be extremely difficult, hence a simplified model is desired. If the time increment of deformation Δt is sufficiently small, enforcement of the Kutta condition can be made arbitrarily close to continuous. If, after each small time increment, the condition of tangency of flow leaving the trailing edge is applied to arrive at a new bound circulation value, then a discrete point vortex will be shed into the wake in a process similar to that modeled by Chow and Huang (Ref. 3). As the deformations continue in time, the above sequence is continuously repeated thus leaving a series of point vortices trailing the airfoil. Figure 3 depicts the previously defined computational model, now with the addition of the circulatory features just described.

In this analysis the flat plate is considered as a limiting case of a symmetrical airfoil whose thickness approaches zero. This avoids the difficulty attendant with infinite velocities that arise at the leading edge of the flat plate. Under the Joukowski transformation

$$z = \zeta + \frac{c^2}{\zeta} \tag{2}$$

where

$$c(t) = a(t) - \varepsilon$$

and

$$\zeta = \zeta' - \varepsilon$$

a circle of radius a in the ζ' plane transforms into a symmetrical airfoil in the z plane.
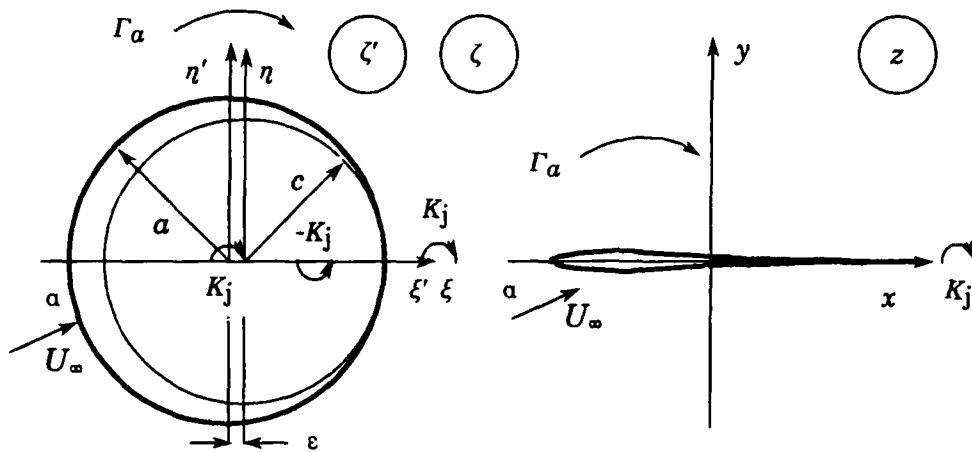
Figure 3. Joukowski transformation of a deforming circular cylinder into a nearly flat plate airfoil at an angle of attack.

If ε is thought of as a thickness parameter then the airfoil thickness will be $O(\varepsilon)$,the leading edge radius is $O(\varepsilon^2)$, and the chord is $4c + O(\varepsilon^2)$ (Ref. 6). The point $\zeta = c$ in the computational plane maps into $z = 2c$ in the physical plane which corresponds to the airfoil trailing edge. Figure 4 provides a more detailed view of the area surrounding the origins of the ζ' and ζ coordinate systems. The limiting process $\varepsilon \to 0$ recovers the flat plate airfoil with the leading edge of zero thickness located at $z = -2c$ in the physical plane. Deformations to the airfoil chord arise entirely through radial deformations of the circular cylinder. Under the transformation of Eq. (2), a freestream of velocity U_∞ in the computational plane maps into the same flow in the physical plane. The circulatory features of the inviscid, incompressible flow are additive to those elements developed in Ref. 4. With the aid of the Circle Theorem (Ref. 7), the resulting complex potential is

written in the fixed ζ plane

$$w(\zeta') = U_\infty \left\{ \zeta' e^{-i\alpha} + \frac{a^2}{\zeta'} e^{i\alpha} \right\} + \frac{i\Gamma}{2\pi} \ln \zeta' + a \frac{da}{dt} \ln \zeta' +$$

$$\sum_{j=1}^{m} \frac{iK_j}{2\pi} \left\{ \ln (\zeta' - \zeta_j') - \ln (\zeta' - \frac{a^2}{\bar{\zeta}_j'}) \right\} \qquad (3)$$

where the overbar denotes the complex conjugate. The first and third terms are, respectively, those for the rigid circular cylinder in a uniform flow and the deforming cylinder as developed in Ref. 4. The second and fourth terms represent the complex
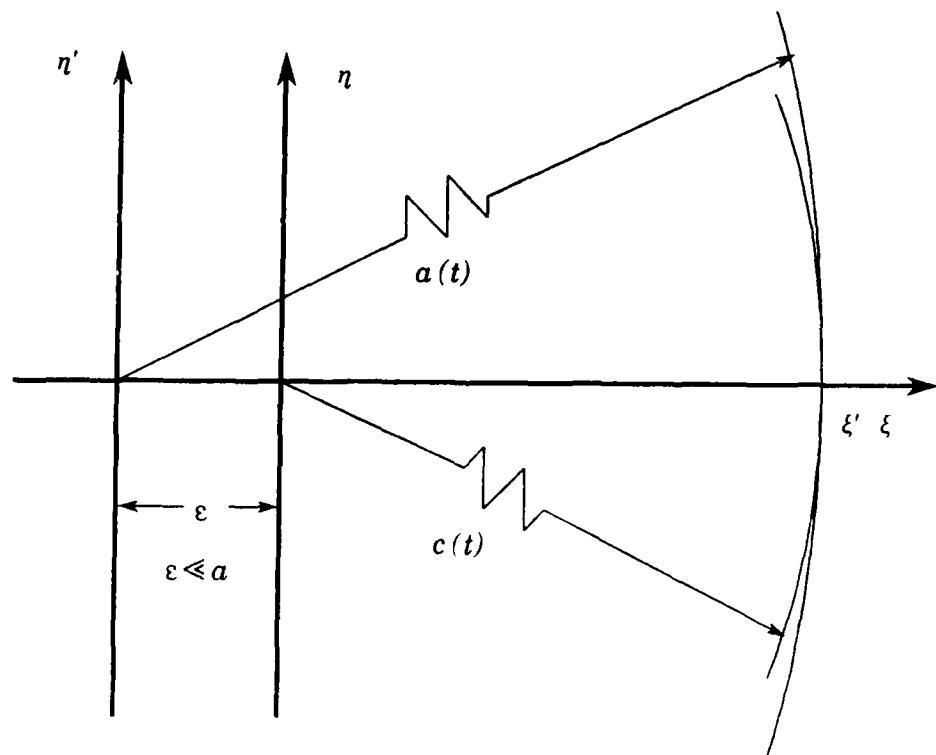
Figure 4. ζ' and ζ coordinate systems in detail. Both systems are fixed.

potential for the circulation bound to the airfoil, Γ_a, as well as the potential for the discrete shed vortices, K_j, and their images within the circle. As was previously accomplished for the elliptical cylinder (Ref. 4), the forces produced by the deformations and the surrounding flow field are determined by the unsteady Blasius Theorem as developed in Ref. 8. The appropriate form for this analysis is given by

$$X + iY = -i\rho z_{TE} \frac{d\Gamma_a}{dt} + \overline{\frac{i\rho}{2} \int_c \left(\frac{dw}{dz}\right)^2 dz} + \frac{d}{dt} \left\{ \rho \frac{d\,Sz_c}{dt} + i\rho \int_c z \frac{dw}{dz}\,dz \right\} \quad (4)$$

X and Y are the resultant forces aligned with the x and y axes of the physical z plane. Γ_a is the vorticity bound to the airfoil and the term Sz_c represents the first moment of area of the airfoil cross-section. The lift and drag are resolved through the transformation

$$D + iL = (X + iY)\,e^{-i\alpha} \quad (5)$$

In terms of the computational coordinate, Eq. (4) is rewritten as

$$X + iY = -i\rho z_{TE} \frac{d\Gamma_a}{dt} + \overline{\frac{i\rho}{2} \int_c \left(\frac{dw}{d\zeta'}\right)^2 / \frac{dz}{d\zeta}\,d\zeta'} + \frac{d}{dt}\left\{ \rho \frac{d\,Sz_c}{dt} + i\rho \int_c z \frac{dw}{d\zeta'}\,d\zeta' \right\} \quad (6)$$

where

$$\frac{dw}{d\zeta'} = U_\infty \left\{ e^{-i\alpha} - \frac{a^2}{\zeta'^2} e^{i\alpha} \right\} + \frac{i\Gamma}{2\pi} \frac{1}{\zeta'} + a \frac{da}{dt} \frac{1}{\zeta'} +$$

$$\sum_{j=1}^{m} \frac{iK_j}{2\pi} \left\{ \frac{1}{\zeta' - \zeta_j} - \frac{1}{\zeta' - \dfrac{a^2}{\bar\zeta_j}} \right\} \quad (7)$$

and

$$\frac{dz}{d\zeta} = \frac{\zeta^2 - c^2}{\zeta^2} \qquad (8)$$

In as much as this is a study of the forces arising from prescribed body deformations, it should be understood that the values for a and da/dt as well as U_∞ and α are input parameters of the problem. Then as posed by Eqs. (6-8), the forces are determined by analysis of the circulation elements of the flow field.

III. The Kutta Condition

In a reference frame fixed to the trailing edge of the airfoil, the complex velocity of the flow, relative to the moving trailing edge, is given by

$$(u - iv)_{TE_{rel}} = \frac{dw}{dz})_{TE_{rel}} = \frac{dw}{d\zeta'})_{\zeta' = a_{rel}} / \frac{dz}{d\zeta})_{\zeta = c} \qquad (9)$$

Since, in the computational plane, the trailing edge is moving to the right at velocity da/dt, then

$$\frac{dw}{d\zeta'})_{a_{rel}} = \frac{dw}{d\zeta'})_{\zeta' = a} - \frac{da}{dt} \qquad (10)$$

where $dw/d\zeta'$ is given by Eq. (7). When Eqs. (7), (8) and (10) are substituted into Eq. (9) and the result is evaluated at the trailing edge, we get

$$(u - iv)_{TE_{rel}} = \left\{ -2iU_\infty \sin \alpha + \frac{i\Gamma}{2\pi a} + \sum_{j=1}^{m} \frac{iK_j}{2\pi} \left[\frac{1}{a - \zeta_j'} - \frac{1}{a - \frac{a^2}{\zeta_j}} \right] \right\} \frac{\zeta^2}{\zeta^2 - c^2})_{\zeta = c} \qquad (11)$$

The resulting infinity at $\zeta = c$ is of course the constraining factor on the bound circulation strength and the individual shed vortex strengths. An indeterminate form exists if the

USAFA-TR-85-11

numerator of Eq. (11) can be set identically to zero such that

$$-2iU_\infty \sin \alpha + \frac{i\Gamma}{2\pi a} + \sum_{j=1}^{m} \frac{iK_j}{2\pi} \left[\frac{1}{a-\zeta_j'} - \frac{1}{a-\frac{a^2}{\overline{\zeta_j'}}} \right] = 0 \qquad (12)$$

For a closed contour that encloses the airfoil and the entire wake, Kelvin's Circulation Theorem requires that, within the contour, the circulation remain constant. Taking this constant value to be that of the circulation required of an airfoil of constant chord $4a_0$ operating under the same flight conditions, then

$$\Gamma_0 = 4\pi U_\infty a_0 \sin \alpha \qquad (13)$$

while the bound circulation Γ_a is found from the constraint

$$\Gamma_0 = \Gamma_a + \sum_{j=1}^{m} K_j \qquad (14)$$

But the circulation strength Γ of Eq. (12) includes both the bound vortex, Γ_a, and that portion of the shed vortex image system located at the origin of the ζ' plane. Thus because

$$\Gamma = \Gamma_a + \sum_{j=1}^{m} K_j$$

and the constraint of Eq. (14), we can say $\Gamma = \Gamma_0$ in Eq. (12). Then the following relationship identically satisfies the Kutta condition and fixes the strength K_m of the mth

9

vortex shed.

$$K_m = \left\{ 4\pi U_\infty (a - a_0) \sin a - \sum_{j=1}^{m-1} K_j \frac{a^2 - \zeta_j' \overline{\zeta_j'}}{(a - \zeta_j')(a - \overline{\zeta_j'})} \right\} /$$

$$\left\{ \frac{a^2 - \zeta_m' \overline{\zeta_m'}}{(a - \zeta_m')(a - \overline{\zeta_m'})} \right\} \qquad (15)$$

ζ_m' is the position, in the computational plane, where the mth vortex is introduced into the flow field. In this analysis, the shed vorticity is assumed to originate in the extended plane of the trailing edge. The distance downstream from the trailing edge for introduction of the vortex is a function of the local velocity evaluated at the trailing edge. This requires only determination of the horizontal velocity component for the case of the flat plate airfoil. Due to the indeterminacy of Eq. (11), the trailing edge velocity is evaluated alternatively as

$$(u - iv)_{TE_{rel}} = \frac{d^2w}{d\zeta'^2} \Big)_{\zeta' = a_{rel}} / \frac{d^2z}{d\zeta^2} \Big)_{\zeta = c} \qquad (16)$$

Another differentiation of Eqs. (7) and (8), with evaluation at the trailing edge, finds the horizontal velocity component to be

$$U_{TE} = \frac{c}{a} U_\infty \cos a + \frac{da}{dt} \left[1 - \frac{c}{2a} \right] - Real \left\{ \frac{c}{4\pi} \sum_{j=1}^{m} iK_j \left[\frac{1}{(a - \zeta_j')^2} - \frac{1}{(a - \frac{a^2}{\overline{\zeta_j'}})^2} \right] \right\} \qquad (17)$$

Then ζ_m' is determined simply from performing the inverse transformation

$$\zeta_m' = \frac{z_m + \sqrt{z_m^2 - 4c^2}}{2} + \varepsilon \qquad (18)$$

on the point

$$z_m = 2c + U_{TE} \Delta t \qquad (19)$$

In practice, Eq. (17) is evaluated prior to the introduction of the mth vortex and actually represents the trailing velocity at the end of the previous time increment. With the shed vortex position now determined, Eq. (15) is used to fix its strength within the Kutta condition requirement of tangent flow at the trailing edge. Note that the strength of this most recently shed vortex is affected by the deformed geometry of the airfoil through its new chord length $4a$. Additionally, the time dependent historical nature of the unsteady problem presents itself through the effects of the previously shed vortices.

IV.   The Resultant Force

The lift produced by the deformations is determined by solution of Eq. (6). An alternative form is written by splitting this relationship into quasi-steady and purely unsteady components. The quasi-steady portion of the Blasius Theorem is written

$$X_1 + iY_1 = \overline{\frac{i\rho}{2} \int_c \left(\frac{dw}{dz}\right)^2 dz} \qquad (20)$$

The phrase quasi-steady here only implies that no explicit time dependence appears in the given terms of the Blasius Theorem. However, since the complex potential has the deformation term in it, a degree of unsteadiness is present even for this apparently steady term. Performing the indicated integrations, one finds that

$$X_1 + iY_1 \sim \left\{ i\rho U_\infty \Gamma - 2\pi\rho U_\infty c \frac{dc}{dt} \right\} e^{i\alpha} - i\rho \sum_{j=1}^{m} K_j \, (u+iv)_{z_j} + \quad O(\varepsilon) \qquad (21)$$

The term $(u + iv)_{z_j}$ in Eq. (21) is the physical plane velocity induced at the jth vortex by all of the other flow elements present and by the singularity images within the circle. A

11

general development of the expression for this induced velocity is included in the Appendix.

For the obviously unsteady contributions from Eq. (4), we're left with

$$X_2 + i\,Y_2 = -i\rho\,z_{TE}\frac{d\Gamma_a}{dt} + \frac{d}{dt}\left\{\rho\frac{d\,Sz_c}{dt} + i\rho\int_c z\frac{dw}{dz}\,dz\right\} \tag{22}$$

The first term on the right, the time rate of change of bound circulation, requires some clarification. If the approximation

$$\left.\frac{d\Gamma_a}{dt}\right)_m \sim \frac{\Gamma_m - \Gamma_{m-1}}{\Delta t} \tag{23}$$

is used, then for the sequence required by the invariance of circulation in the global sense

$$\Gamma_0 = \Gamma_1 + K_1 \qquad \Rightarrow \qquad \Gamma_1 - \Gamma_0 = -K_1$$

$$\Gamma_0 = \Gamma_2 + K_1 + K_2 \qquad \Rightarrow \qquad \Gamma_2 - \Gamma_0 = -K_1 - K_2$$

$$\Gamma_2 - \Gamma_1 = -K_2 \tag{24}$$

$$\Gamma_m - \Gamma_{m-1} = -K_m$$

we get

$$\left.\frac{d\Gamma_a}{dt}\right)_m \sim -\frac{K_m}{\Delta t} \tag{25}$$

Equation (25) is merely a statement that the instantaneous rate of bound circulation

change is equal to the strength of the most recently shed vortex divided by the time increment.

The second term from Eq. (22) is evaluated even for the present case, since the flat plate is expected to be recovered only in the limit $\varepsilon \to 0$. For non-zero values of ε, the first moment of the area, Sz_c, and its time derivatives are expectedly non-zero and are evaluated as follows.

If the area is defined as the surface integral

$$S = \int\int_S dx\,dy$$

then application of Green's Theorem in its complex form (Ref.9)

$$\int\int_S \frac{\partial F}{\partial \bar{z}}\,dx\,dy = -\frac{i}{2}\int_c F(z,\bar{z})\,dz \qquad (26)$$

results in, for the profile cross-sectional area

$$S = -\frac{i}{2}\int_c \bar{z}\,dz \qquad (27)$$

C is now the closed contour defining the airfoil perimeter. Similarly, for the first moment of the area as defined by the surface integral

$$S z_c = \int\int_S z\,dx\,dy$$

utilization of Eq. (26) produces

$$S z_c = -\frac{i}{2}\int_c z\,\bar{z}\,dz \qquad (28)$$

For the first moment of area, evaluation of Eq. (28) gives, through first order in ε

$$S z_c = -2 \pi c^2 \varepsilon + O(\varepsilon^2)$$

Evaluation of Eq. (21) as ε → 0 results in

$$X_2 + i\,Y_2 \sim i\rho\,2c\,\frac{K_m}{\Delta t} + i8\pi\rho\,U_\infty c\,\frac{dc}{dt}\sin a + i\rho\sum_{j=1}^{m} K_j\,\frac{d}{dt}\left[\frac{c^2}{\dot{\zeta}_j} + \frac{\bar{c}^2}{\dot{\bar{\zeta}}_j}\right] + O(\varepsilon) \quad (29)$$

Together, Eqs. (21) and (29) constitute the solution for the "near" flat plate that is undergoing chord deformations. For the limiting case where ε→0, Eq. (21) and (29) are equivalent to the results achieved by Sarpkaya (Ref. 10), who analyzed an inclined flat plate of constant chord without bound circulation. Sarpkaya assumed a Kutta condition at both the leading and trailing edges that resulted in finite velocities at both ends. In effect, the present analysis assumes a finite velocity to occur at the leading edge because of its extremely small, but non-zero, radius of curvature. Finiteness of ailing edge velocity is insured in the traditional manner through enforcement of the Kutta condition. Because the velocity remains finite at the leading edge, the paradox of Cisotti (Ref. 11) does not appear in the current study.

For the purely steady case, in which no chord deformations occur, no discrete vortices are shed as per Eq. (15). Thus only the first steady term from Eq. (21) would remain and the lift predicted by the Kutta -Joukowski Theorem is recovered.

If the lift and drag are normalized by the steady state lift that is generated by the original airfoil geometry, then the relative effects of the deforming airfoil can be determined. If this steady lift is that derived from the Kutta-Joukowski Theorem, then,

for the original airfoil geometry, it is given by

$$L_0 = \rho \, U_\infty \Gamma_0$$

where, from Eq. (13)

$$\Gamma_0 = 4 \, \pi \, U_\infty a_0 \, \sin \alpha$$

Then the lift and drag information derived from the previous analysis is displayed in its normalized form

$$\frac{D + i \, L}{L_0} \qquad\qquad (30)$$

In this form, however, the forces arising from the unsteadiness of the actual deformations as well as the steady forces arising from the newly deformed geometry are not separable. These two contributions become decoupled when the computed lift and drag are normalized by the steady lift that would be achieved by the airfoil in its deformed state. Now the normalization is accomplished in the form

$$\frac{D + i \, L}{L_s} \qquad\qquad (31)$$

where

$$L_s = \rho \, U_\infty \Gamma_s$$

and

$$\Gamma_s = 4 \, \pi \, U_\infty a \, \sin \alpha$$

Effectively, in the case of the flat plate, the only difference in the two normalization

schemes is that the second method incorporates the deformed chord.

Computationally, the lift is determined at each time step as follows. For a specified chord deformation rate/freestream velocity ratio (EVR) and time step, the new chord length is determined. As discussed earlier, due to the newly deformed geometry, the original circulation must be increased by an amount sufficient to maintain tangential flow at the trailing edge. A discrete vortex is shed at the end of the deformation whose position is fixed by evaluation of Eq. (17) for the trailing edge velocity and substitution of this value into Eq. (19). The most recently shed vortex strength is then determined by solution of Eq. (15). The complex velocities of each of the shed wake vortices are computed as described in the Appendix and used in Eqs. (21) and (29) to find the instantaneous resultant forces. Through the transformation of Eq. (5), the lift resulting from the deformations is determined and then normalized by Eqs. (30) and (31). The wake vortices' new positions in the flow are determined as discussed in the Appendix. The trailing edge velocity is evaluated, and another prescribed deformation occurs. The newest vortex is introduced into the wake and the computational process is repeated.

V.   Results and Conclusions

Figures 5 and 6 provide graphical description of the lift enhancement derived from different chord deformation rates.   Figure 5 shows the imaginary component of Eq. (30) for an angle of attack of $8°$. The curves shown here are representative of those for all practical angles of attack. Because of the normalization process, the angle of attack dependence of the L/L_0 is effectively removed for angle of attack generally less than $15°$. For greater angles of attack at larger EVR values, the closer proximity of stronger discrete vortices in the wake tends to give slight normalized lift variation with angle of attack. The normalization of lift values given in Fig. 5 shows that one obvious effect of chord stretching is an increase in generated lift. This manner of data presentation, however,
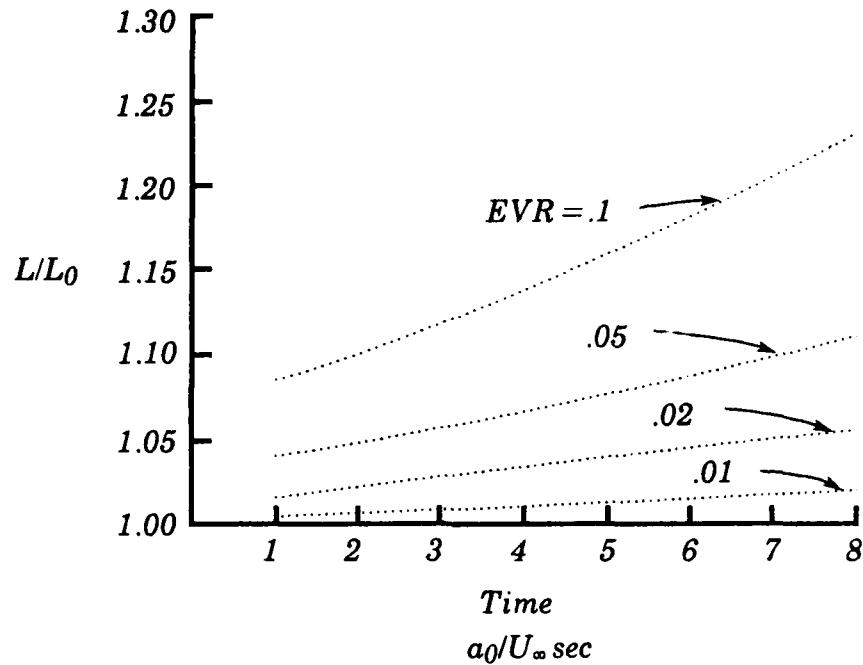
Figure 5. Unsteady L/L_0 ratio generated by a flat plate airfoil
undergoing chord stretching. $a=8°$

combines those lift enhancement features resulting from both the new geometry and

the unsteadiness that produces the new geometry. The normalization of Eq. (30) does

provide an accurate time history of the expected lift enhancement that would result

from chord stretching. The results cited in Ref. 4 indicated that larger EVR values resulted

in more favorable lift enhancement. Figure 5 verifies that characteristic, but in this case,

for a body with circulation based lift dominating.

Figure 6 provides a view of the purely unsteady effects that are derived from the

chord stretching. Because the normalization of Eq. (31) also effectively removes the

angle of attack dependence, the curves shown for an angle of attack of $8°$ are

representative of those for all practical angles of attack. The earlier discussion about

greater angles of attack with large *EVR* values still applies. The curves indicate that chord stretching itself provides an unsteady increment to the lift. The more rapidly the chord is made to stretch, the larger is the increment. The time behavior of this normalized lift shows that the unsteady contribution becomes a proportionally smaller part of the overall lift generation. This results from the fact that the total lift developed by the deformations is continuously normalized by a "steady" lift value that increases with time.
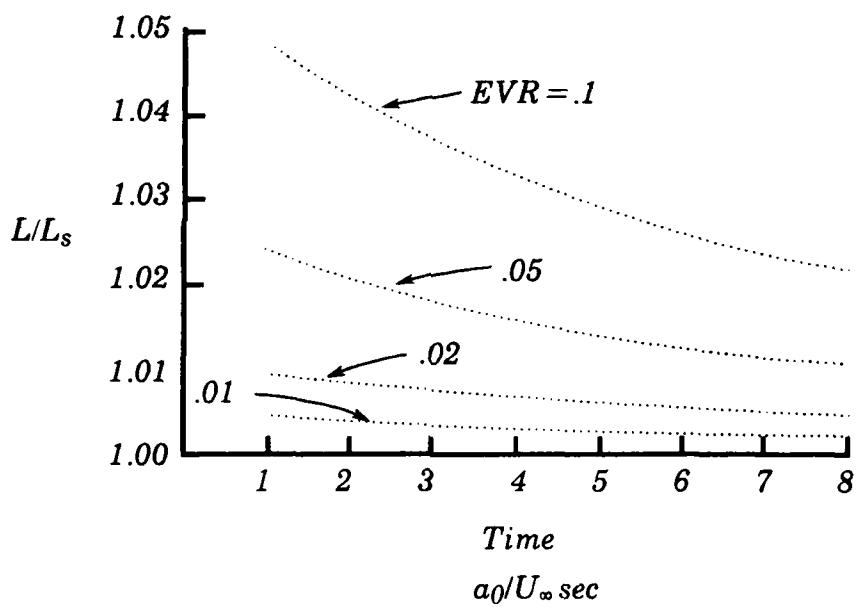

Figure 6. Unsteady L/L_s ratio generated by a flat plate airfoil undergoing chord stretching. $\alpha = 8^\circ$

References

1. McCroskey, W. J., "Unsteady Airfoils," Annual Review of Fluid Mechanics, Vol. 14, edited by Van Dyke, M., Wehausen, J. V., and Lumley, J. L., Annual Reviews Inc., Palo Alto, 1982, pp. 285-311.

2. Walker, J., Helin H., and Chou D., "Unsteady Surface Pressure Measurements," AIAA Paper 85-0532, Mar 1985.

3. Chow, C. Y., and Huang, M. K., "Unsteady Flows About a Joukowski Airfoil in the Presence of Moving Vortices," AIAA Paper 83-0129, Jan. 1983.

4. Russell, J.H., and Chow, C.Y., "Unsteady Forces on an Elliptical Cylinder Undergoing Time Dependent Geometrical Changes," Aeronautics Digest, USAFA TR-84-7, September 1984.

5. McCroskey, W. J., "Some Current Research in Unsteady Fluid Dynamics," Journal of Fluids Engineering, Vol. 99, Mar. 1977, pp.8-38.

6. Karamcheti, K., Principles of Ideal - Fluid Aerodynamics, 1st ed., Krieger Pub. Co., Malabar, Fl., 1980, Sec. 16.9.

7. Milne-Thompson, L. M., Theoretical Hydrodynamics, 4th ed., Macmillan, New York, 1960, Sec. 13.50.

8. Sedov, L. I., Two-Dimensional Problems in Hydrodynamics and Aerodynamics, 1st ed., Wiley, New York, 1965, Sec. 1.3.

9. Spiegel, M. R., Complex Variables, 1st ed., McGraw Hill, New York, 1964, p. 95.

10. Sarpkaya, T., "An Inviscid Model of Two-Dimensional Vortex Shedding for Transient and Asymptotically Steady Separated Flow Over an inclined Plate," Journal of Fluid Mechanics, Vol. 68, 1975, pp. 109-128.

11. Birkhoff, G., Hydrodynamics, Revised ed., 2nd ed., Univ. Press, Princeton, 1960, Sec. 1.8.

12. Milne-Thompson, L. M., Ibid., p.355.

13. Giesing, J. P.,"Nonlinear Two-Dimensional Unsteady Potential Flow With Lift," Journal of

Aircraft, Vol. 5, Mar.-Apr. 1968, pp. 135-143.

APPENDIX

THE MOTION OF THE DISCRETE VORTEX WAKE

This analysis has shown that the forces arising from the unsteady deformations of an airfoil require evaluation of the velocities induced at each of the discrete vortex centers. From Milne-Thompson (Ref. 12), the complex velocity induced at the nth vortex by all of the other elements of the flow field is given by

$$(u - iv)_{z_n} = \lim_{z \to z_n} \frac{d}{dz} \left\{ w - i \frac{K_n}{2\pi} \ln(z - z_n) \right\} \qquad (A.1)$$

Here, w(z) is the complex potential of all of the flow elements including the discrete vortices and their associated image systems as shown in Fig.A.1. Equation (A.1) is written alternatively as

$$(u - iv)_{z_n} = \lim_{\zeta' \to \zeta_n} \left\{ \frac{dw}{d\zeta'} \bigg/ \frac{dz}{d\zeta} - i \frac{K_n}{2\pi} \frac{1}{z - z_n} \right\} \qquad (A.2)$$
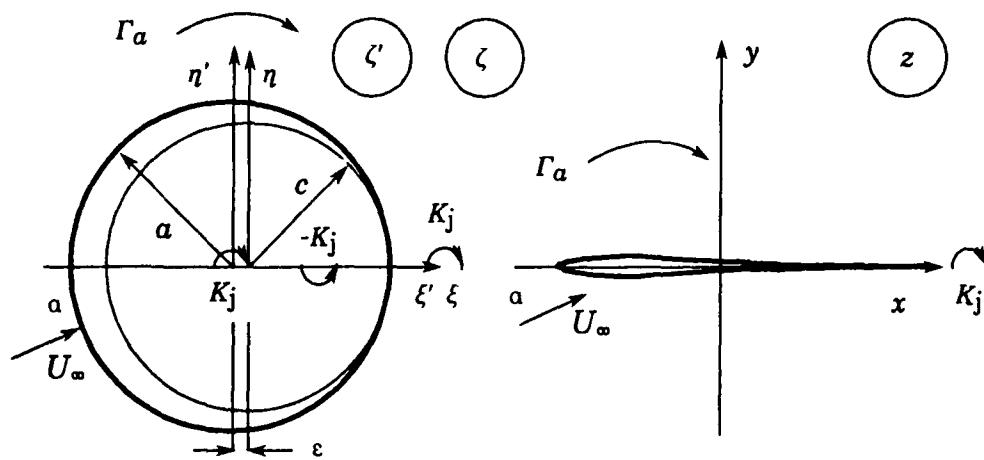
Figure A.1. Joukowski transformation of a deforming circular cylinder into a nearly flat plate airfoil at an angle of attack.

Then for

$$w(\zeta') = U_\infty \left\{ \zeta' e^{-i\alpha} + \frac{a^2}{\zeta'} e^{i\alpha} \right\} + \frac{i\Gamma}{2\pi} \ln \zeta' + a \frac{da}{dt} \ln \zeta' +$$

$$\sum_{j=1}^{m} \frac{iK_j}{2\pi} \left\{ \ln(\zeta' - \zeta_j') - \ln(\zeta' - \frac{a^2}{\overline{\zeta_j'}}) \right\}$$

Equation (A.2) becomes

$$
(u-iv)_{z_n} = \left\{ U_\infty \left[e^{-i\alpha} - \frac{a^2}{\zeta_n'^2} e^{i\alpha} \right] + \frac{i\Gamma}{2\pi} \frac{1}{\zeta_n'} + a\frac{da}{dt}\frac{1}{\zeta_n'} - \right.
$$

$$
\sum_{j=1}^{m} \frac{iK_j}{2\pi} \left[\frac{1}{\zeta_n' - \dfrac{a^2}{\overline{\zeta_j'}}} \right] + \sum_{j\neq n}^{m} \frac{iK_j}{2\pi} \left[\frac{1}{\zeta_n' - \zeta_j'} \right] \Bigg\} \frac{\zeta_n^2}{\zeta_n^2 - c^2} +
$$

$$
\lim_{\zeta' \to \zeta_n'} i\frac{K_n}{2\pi} \left\{ \frac{1}{\zeta' - \zeta_n'}\frac{d\zeta'}{dz} - \frac{1}{z - z_n} \right\} \qquad (A.3)
$$

Evaluation of the first and largest bracket term is straightforward for the known positions of the vortex centers. The second bracketed quantity of Eq. (A.3) is analyzed by assuming that the term within the brackets can be expanded in a Taylor series about the point ζ_n'. Thus

$$
\frac{d\zeta'}{dz} = \left(\frac{d\zeta'}{dz} \right)_{\zeta_n'} + (\zeta' - \zeta_n')\frac{d}{d\zeta'}\left\{ \frac{1}{\dfrac{dz}{d\zeta'}} \right\}_{\zeta_n'} + O(\zeta' - \zeta_n')^2
$$

which then becomes

$$
\frac{d\zeta'}{dz} = \left(\frac{d\zeta'}{dz} \right)_{\zeta_n'} - (\zeta' - \zeta_n')\left(\frac{d^2 z}{d\zeta'^2} \right)_{\zeta_n'}\left(\frac{d\zeta'}{dz} \right)_{\zeta_n'}^2 + O(\zeta' - \zeta_n')^2 \qquad (A.4)
$$

For the term $1/(z-z_n)$, consider first the expansion

$$z - z_n = (\zeta' - \zeta'_n)\left(\frac{dz}{d\zeta'}\right)_{\zeta'_n} + \frac{(\zeta' - \zeta'_n)^2}{2}\left(\frac{d^2z}{d\zeta'^2}\right)_{\zeta'_n} + O(\zeta' - \zeta'_n)^3 \quad \text{(A.5)}$$

If the reciprocal of both sides of Eq. (A.5) is taken, it becomes

$$\frac{1}{z - z_n} = \frac{1}{(\zeta' - \zeta'_n)\left(\dfrac{dz}{d\zeta'}\right)_{\zeta'_n} + \dfrac{(\zeta' - \zeta'_n)^2}{2}\left(\dfrac{d^2z}{d\zeta'^2}\right)_{\zeta'_n} + O(\zeta' - \zeta'_n)^3} \quad \text{(A.6)}$$

Applying the Binomial Theorem to Eq. (A.6) results in

$$\frac{1}{z - z_n} = \frac{1}{\zeta' - \zeta'_n}\left(\frac{d\zeta'}{dz}\right)_{\zeta'_n} - \frac{1}{2}\left(\frac{d^2z}{d\zeta'^2}\right)_{\zeta'_n}\left(\frac{d\zeta'}{dz}\right)^2_{\zeta'_n} + O(\zeta' - \zeta'_n) \quad \text{(A.7)}$$

If Eqs. (A.4) and (A.7) are combined, then the second bracketed term in Eq. (A.4) becomes

$$\lim_{\zeta' \to \zeta'_n} i\frac{K_n}{2\pi}\left\{\frac{1}{\zeta' - \zeta'_n}\frac{d\zeta'}{dz} - \frac{1}{z - z_n}\right\} = i\frac{K_n}{2\pi}\left\{-\frac{1}{2}\left(\frac{d^2z}{d\zeta'^2}\right)\left(\frac{d\zeta'}{dz}\right)^2\right\}_{\zeta'_n} \quad \text{(A.8)}$$

For the Joukowski transformation

$$z = \zeta + \frac{c^2}{\zeta}$$

the limiting value of Eq. (A.8) is then found to be

$$-i\frac{K_n}{2\pi}\frac{\zeta_n c^2}{(\zeta_n^2 - c^2)^2} \qquad\qquad (A.9)$$

Combining all of the terms, the velocity induced at the nth vortex becomes

$$(u - i v)_{z_n} = \left\{ U_\infty \left[e^{-i\alpha} - \frac{a^2}{\zeta_n'^2} e^{i\alpha} \right] + \frac{i\Gamma}{2\pi}\frac{1}{\zeta_n'} + a\frac{da}{dt}\frac{1}{\zeta_n'} - \right.$$

$$\left. \sum_{j=1}^{m} \frac{iK_j}{2\pi}\left[\frac{1}{\zeta_n' - \dfrac{a^2}{\overline{\zeta_j'}}} \right] + \sum_{j\neq n}^{m} \frac{iK_j}{2\pi}\left[\frac{1}{\zeta_n' - \zeta_j'} \right] \right\} \frac{\zeta_n^2}{\zeta_n^2 - c^2} -$$

$$i\frac{K_n}{2\pi}\frac{\zeta_n c^2}{(\zeta_n^2 - c^2)^2} \quad (A.10)$$

The induced velocity, determined by solution of Eq. (A.10), is then used in the computation of the unsteady aerodynamic forces resulting from the deformations.

With time, the point vortices are swept away from the airfoil as though they were fluid particles. The trajectory of each vortex center is determined by using the predictor-corrector integration scheme of Giesing (Ref. 13). If $z(t_0)$ represents the position of the nth vortex in the physical plane at time t_0, then the predictor step of the integration scheme places the new position z_p at

$$z_p = z(t_0) + \overline{\left\{ u[z(t_0)] - i v[z(t_0)] \right\}}\Delta t$$

where the overbar denotes the complex conjugate. The velocity induced at this new

25

predicted point is computed and the final, corrected position at time $t_0 + \Delta t$ is found from

$$z(t_0 + \Delta t) = z(t_0) + \frac{1}{2} \overline{\left\{ u[z(t_0)] - i v[z(t_0)] + u[z_p] - i v[z_p] \right\}} \Delta t$$

Far from the airfoil, the dominant term in the induced velocity relationship becomes the freestream flow, which remains constant with time, and the effects of the closest neighboring vortices. Figure A.2 depicts the typical wake trajectory for the case where the prescribed deformations result in an increase in bound circulation.

U_∞
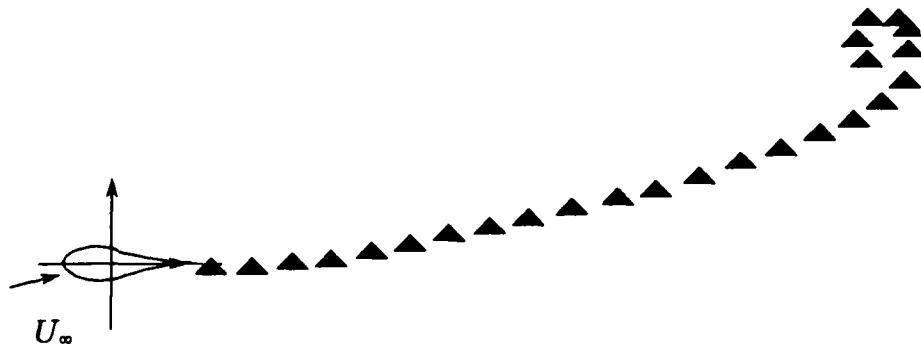
Figure A.2. Discrete vortex trajectory for typical deformation that resulted in increase in bound circulation.

This case represents the generally favorable one from a lift enhancement point of view and the wake is shown to roll up as expected. It was determined that for all practical purposes, the wake itself provided little interaction with the freestream,

circulation and deformation dominated flow field.

Unsteady Surface Pressure Measurements On A Pitching Airfoil

John M. Walker* Henry E. Helin ** and David C. Chou***

Abstract

Surface pressure measurements were taken in an experimental investigation of the energetic dynamic stall vortices and the associated unsteady aerodynamics generated by and surrounding a 6-in. NACA 0015 airfoil pitching at high rates to large amplitudes. The airfoil was pitched at rates from $230°$/sec to $1380°$/sec and amplitudes from $0°$ to $60°$ about its quarter-chord axis. Pitch rate, Reynolds number, and the non-dimensional pitch rate, $a+$, were varied to study the effects on pressure and lift coefficients. The experimenters found that increases in pitch rate and Reynolds number had inverse effects on the flow field in the immediate vicinity of the airfoil ; consequently, the maintenance of a constant non-dimensional pitch rate produced very similar results.

I.   Introduction

As pointed out by McCroskey, (Ref. 1) the energetic nature of the unsteady flowfields

has been a topic of study for most of the twentieth century. Because of their

complicated, rapidly changing time dependent nature , only recently has significant

progress been made in theoretical and experimental efforts to understand the fluid

mechanics of these flowfields. A particular unsteady flow phenomenon, dynamic stall

has become increasingly important because of the need not only to predict its onset but

also to understand its active nature and exploit the associated increases in aerodynamic

coefficients. The importance of the former has been well known for years with regard to

helicopter rotors, turbo-machinery, and vertical axis wind turbines. A large part of the

---

* Major, USAF, Chief, Aeromechanics Division, Frank J. Seiler Research Lab., USAF Academy, CO.
** 1st Lt, USAF, PhD student , Univ. of Colorado, Boulder, CO.
*** Professor of Mechanical Engineering, University of New Mexico, Albuquerque, NM.

latter has received impetus from Herbst (Ref. 2) who studied the "supermaneuverability" of fighter aircraft. Understanding of highly unsteady flowfields has been hampered by two factors: 1) the absence of accurate analytical methods - short of full Navier-Stokes solutions which are only now becoming viable - to predict these flowfields and 2) a lack of experimental data needed to set modeling parameters and to verify theoretical calculations.

Most of the experimental data on unsteady flows about pitching airfoils to date have been restricted to sinusoidally oscillating models undergoing relatively small amplitude motions (up to ± 10°) about relatively low mean angles of attack (0° - 15°). These are typified by the experiments of McCroskey and Philippe (Ref.3), McAlister and Carr (Ref. 4), Martin, et. al.(Ref. 5), and Robinson and Luttges(Ref.6). These data, including flow visualization, hot-wire, and pressure measurements, are applicable to many fluid devices of importance. With the exception of Robinson and Luttges (Ref.7), however, these studies have not focused on the fact that the extremely energetic nature of the unsteady flowfields could be used to enhance performance. Carr, et. al. (Ref.8) have shown that lift, drag, and moment coefficients associated with unsteady flowfields greatly exceed their static counterparts. However, a limited amount of experimental data have been obtained from the very large amplitude motions that will be required if the maneuvers proposed by Herbst (Ref.2) using angles of attack in excess of 45° are to be implemented.

Studies of moderate to large amplitude constant rate motions have been performed by Harper and Flanigan (Ref. 9), who obtained force balance data on a small model pitching up to 30°, Francis, et. al. (Ref.11), who obtained surface pressure measurements on airfoils pitching up to 60°, Deekins and Kuebler (Ref.12), who obtained flow visualization of dynamic leading edge separation at low Reynolds numbers in a

smoke tunnel, Daley (Ref. 13), who obtained leading edge dynamic stall data at low Reynolds numbers, and Walker, et. al. (Ref. 14) and Helin and Walker(Ref. 15), who obtained flow visualization using a smoke-wire and near surface hot-wire velocity magnitude data on an airfoil pitching up to $60°$. Clearly, an extensive amount of experimental effort needs to be performed to obtain a clear understanding of the fluid dynamic mechanisms precipitating the occurrence of the dynamic vortices associated with the unsteady flowfields surrounding airfoils pitching at high rates to large amplitudes. This experimental effort intends to add to that understanding by exploring a well defined but limited parameter range of pitch rates and Reynolds numbers.

II.   Experimental Arrangement

All data were obtained in the USAF Academy Aeronautics Laboratory low-speed, *2 ft x 3 ft* subsonic wind tunnel. The model used was a full span, 6 inch chord, NACA 0015 airfoil. The airfoil was instrumented with eighteen Endevco 8507-2 miniature pressure transducers close-coupled to the surface ports, as shown in Fig. 1. The signals from each transducer were amplified through Dynamics 7512B amplifiers. The pitching motions of the airfoil were generated by a PDP 11/03 computer, which commanded a Control Systems Research Index-Syn stepper motor/driver system. This is a modified version of the two-degree-of-freedom oscillator developed by Francis, et. al. (Ref. 16). The PDP 11/03 was slaved to a PDP 11/45, which performed the supervisory control and data acquisition. Since the airfoil motions were very repeatable, all eighteen pressure ports were located on one side of the airfoil for better data resolution. This resulted in some minor errors in the data between the upper and lower surfaces due to difficulties in returning the tunnel to the precise flow speed for the opposite surface after turning the airfoil over. The reversal of the airfoil was necessitated by the fact that the stepping motor would turn in only one direction.
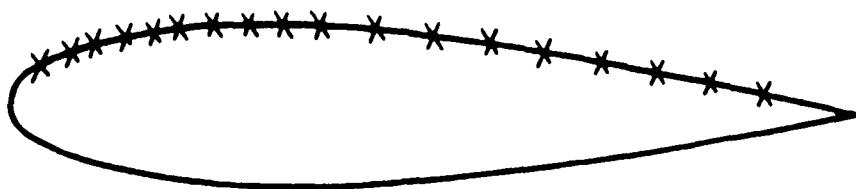
Figure 1. Pressure Port Locations

Experiments were conducted employing a variety of constant rate pitching motions and flow speeds. Table 1 shows the experimental matrix with $\dot{\alpha}$ given in *deg/sec* and U_∞ in *ft/sec*, and with the interior values given by the non-dimensional pitch rate parameter $a^+ = \dot{\alpha}\,c/U_\infty$. All of the motions were performed by pitching the airfoil from angles of attack of zero degrees to sixty degrees and then stopping the motion. See Fig. 2.

Table 1

$\dot{\alpha}$ (°/s)

	230	460	920	1380
U_∞ (f/s)				
20	0.1	0.2	0.4	0.6
40	---	0.1	0.2	---
60	---	---	---	0.2
80	---	0.05	0.1	---

The Reynolds number based on chord varied from 47500 to 190000. The major objectives of these experiments were to examine the effects of varying pitch rate at constant Reynolds number, varying Reynolds number at constant pitch rate, and holding a^+ constant while varying both pitch rate and Reynolds number. For the nine cases shown in Table 1, data were taken for both surfaces of the airfoil by performing twenty-
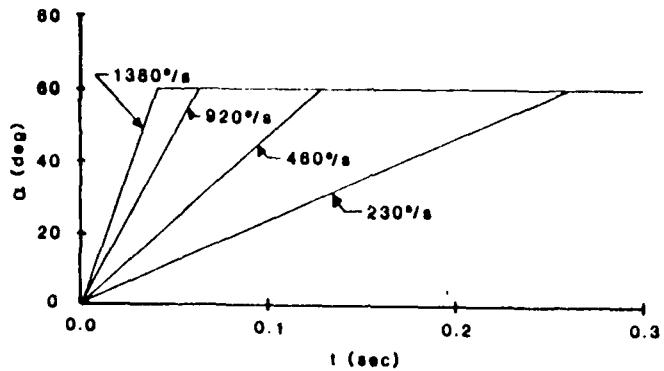
Figure 2. Angle of attack versus time

five repetitions of the pitching motions, taking *200* data points per sensor, and taking the ensemble average.

III.   Experimental Results

The objectives of these experiments were to examine the unsteady aerodynamics surrounding a pitching airfoil and the time dependent fluid mechanics associated with varying pitch rate, Reynolds number, and the non-dimensional pitch rate parameter, a^+. The matrix, shown in Table 1 above, was designed to accomplish this task within the experimental constraints of the control, instrumentation, and data acquisition system. The pressure data were used to calculate pressure coefficients which were in turn integrated to compute lift coefficients. Both types of curves were plotted in the usual way: C_p *vs* x/c and C_l *vs* a. Since these experiments were limited to a single airfoil, varying the Reynolds number was synonymous with varying the flow velocity in the tunnel.

A.   Section Lift Coefficient versus Alpha

The effect of varying the pitch rate while holding Reynolds number constant was dramatic, particularly at the lower flow velocities. At *Re = 47500*, C_{lmax} was a strong function of pitch rate, varying from *2* to *4.3* as pitch rate was increased from *230 deg/s* to *1380 deg/s*. At this Reynolds number, dC_l/da was also a strong function of pitch rate,

varying from *4.3/rad* to *8/rad*. As Reynolds number increased to *95000* and *190000*, however, their dependence is less pronounced. Fig. 3 shows C_l vs a for various pitch rates at three different Reynolds numbers, and Fig. 4 shows the effect on C_{lmax} of increasing pitch rate at constant *Re*.
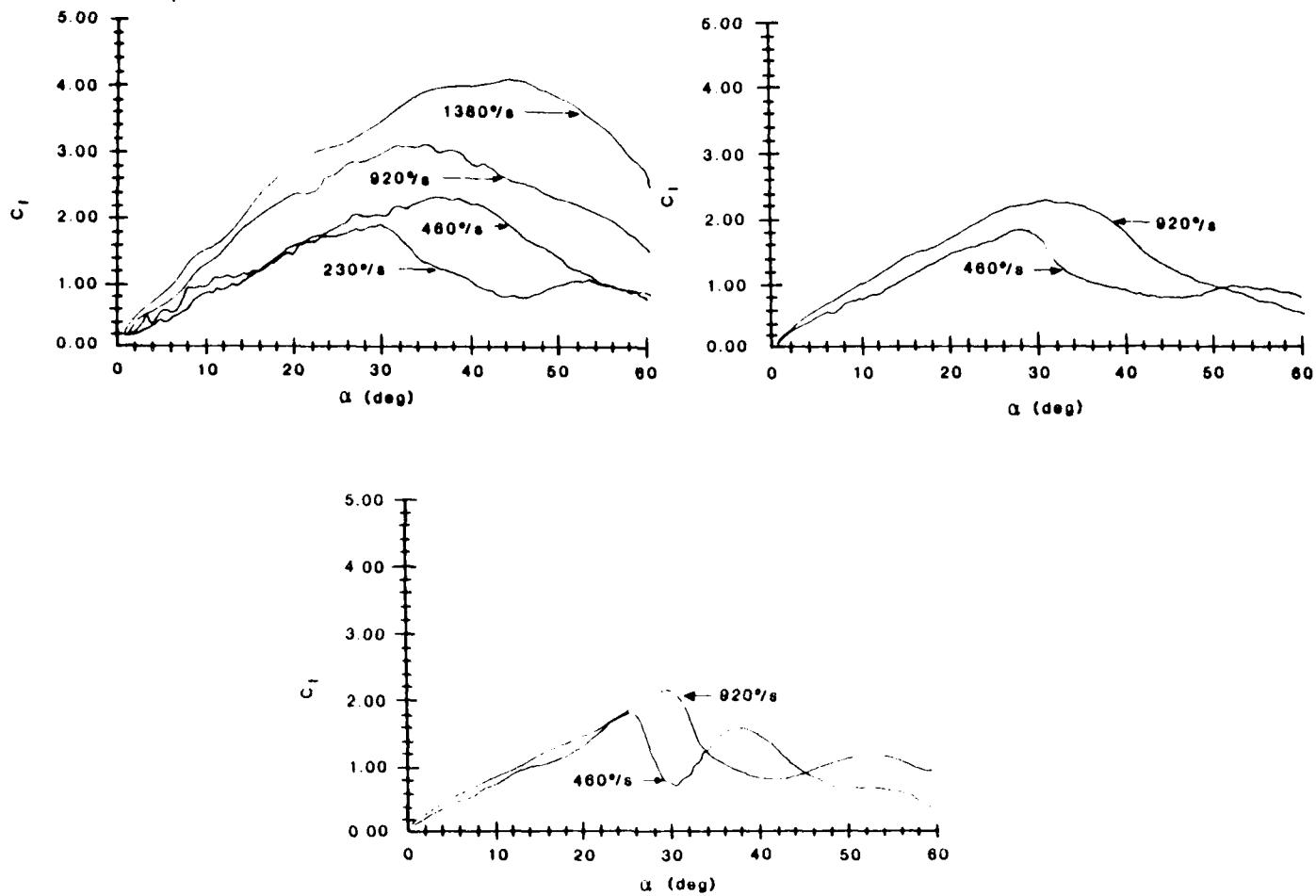
Figure 3. C_1 vs a for constant U_∞ at various pitch rates

Fig. 4 shows (from Figure 3(a) only) a somewhat linear increase in C_{lmax} with respect to pitch rate. Gormont (Ref. 17) and Strickland and Graham (Ref. 18) have shown a square root dependency on non-dimensional pitch rate for inception of dynamic stall. Gormont also shows a similar correlation for lift stall. Also, Walker, et. al. (Ref. 14) and Helin and Walker (Ref. 15) presented near-surface hot-wire data that, while being impossible to
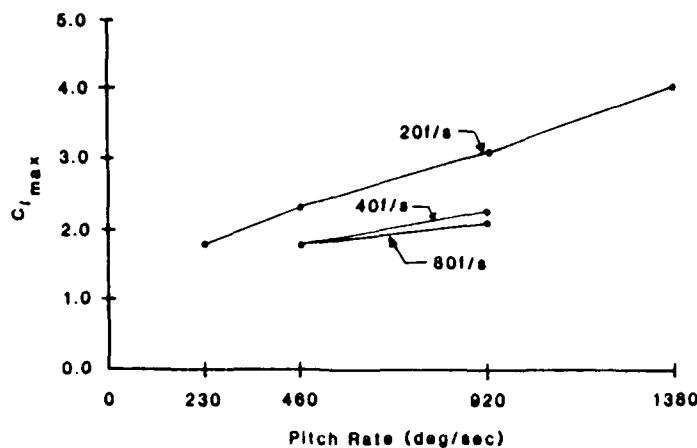
Figure 4. C_{1max} vs α at various Reynolds number

calculate lift coefficients from, indicates support for this conclusion. While for steady flows, a direct correlation exists between C_{lmax} and stall, interestingly, for these types of unsteady flows, the correlation is not straightforward. In addition to the effect of pitch rate on C_{lmax}, there is a general dependence of the slope of the lift curve and of the angle of attack at which C_{lmax} occurs; and again, this dependence is less pronounced as Reynolds number increases.

The effect of varying Reynolds number while holding pitch rate constant is rather the opposite. C_{lmax} is reduced significantly when increasing Reynolds number from 47500 to 95000 or 1425000, but is only slightly affected by increasing Re from 95000 to 190000. Fig. 5 shows C_l vs α for various Reynolds numbers at three different pitch rates, and Fig. 6 shows the effects of C_{lmax} of increasing Re at constant pitch rate. The angle of attack at which C_{lmax} occurs is also inversely dependent on Reynolds number, as is $dC_l/d\alpha$ for rotation rates of 920 an 1380 deg/s. Oddly enough, however, the lift curve slopes at the pitch rate of 460 deg/s are all much the same.
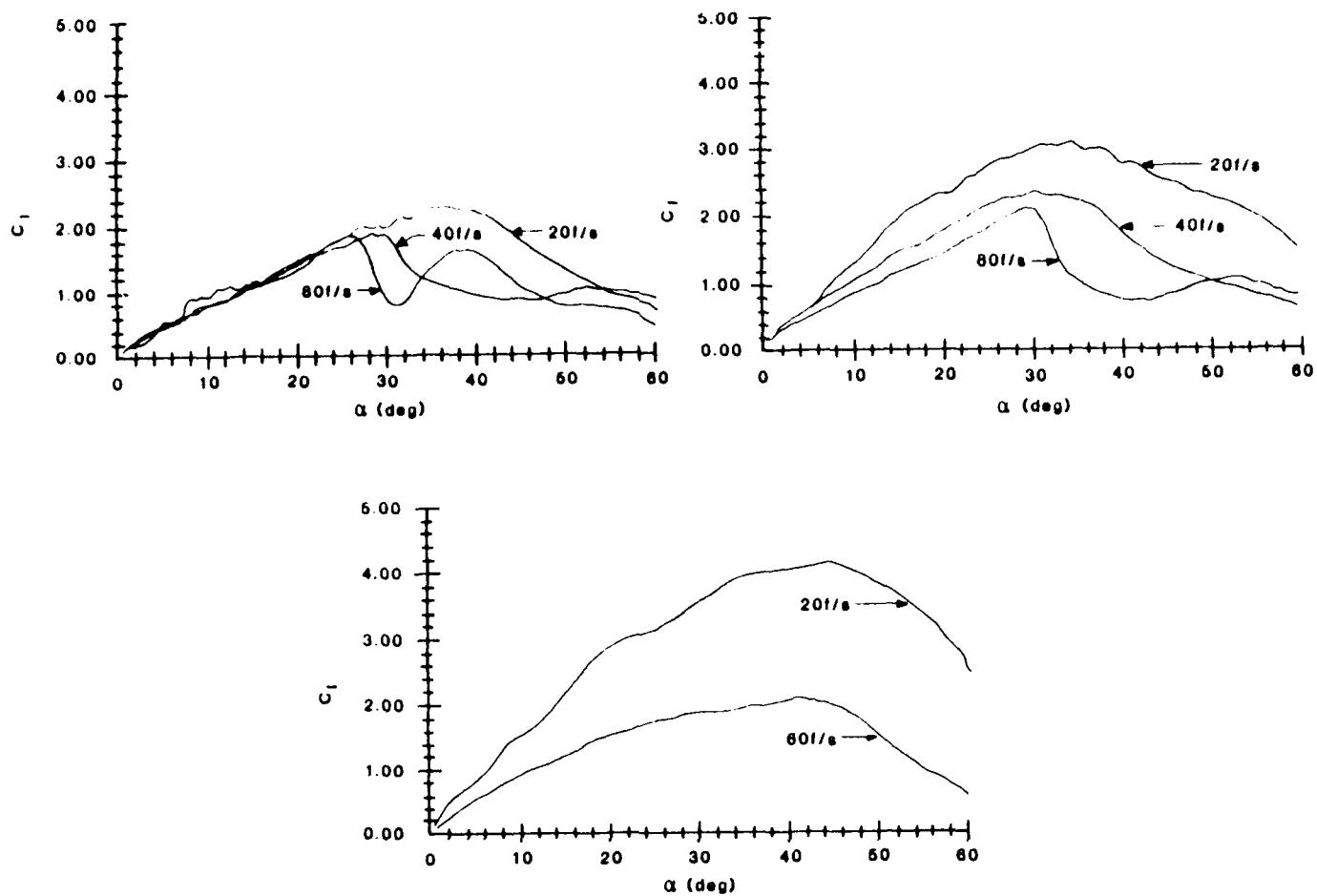
Figure 5. C_1 vs α at constant pitch rate for various U_∞
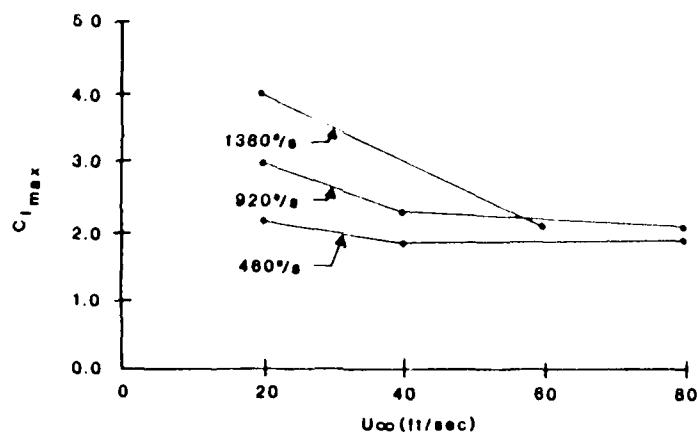
Figure 6. C_{1max} vs U_∞ at various pitch rates

The effect of maintaining the non-dimensional pitch rate parameter, a^+, constant within the range of Reynolds numbers investigated here is of special significance. Two cases were studied: that of $a^+ = 0.1$ and $a^+ = 0.2$. As can be seen from Table 1, these were obtained by increasing both pitch rate and flow velocity proportionately. Figs. 7 and 8 show C_l vs a curves for the respective constant cases.
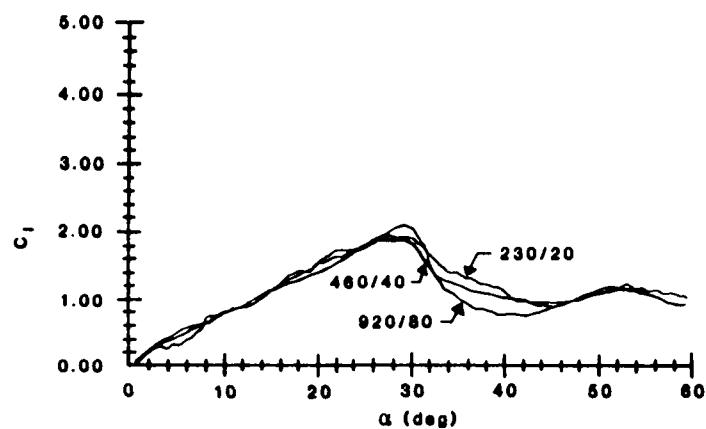
Figure 7. $a^+ = 0.1, \dot{a} = 230, 460, 920$ deg/sec, $U_\infty = 20, 40, 80$ ft/sec
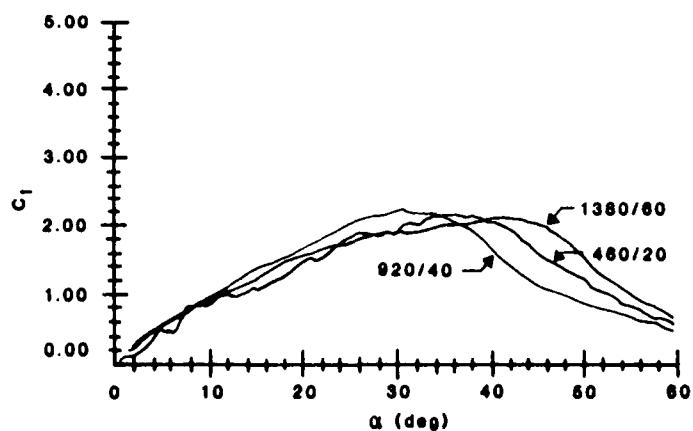
Figure 8. $a^+ = 0.2, \dot{a} = 460, 920, 1380$ deg/sec, $U_\infty = 20, 40, 80$ ft/sec

As one can readily see, each set of constant α^+ curves are very similar. For $\alpha^+ = 0.1$, each of the three curves start out at a high initial slope for the first two or three degrees, then proceed linearly at a slope of approximately 4.2 until reaching a C_{lmax} of about 2.0 at 31 or 32 degrees. The higher pitch rates produce slightly higher values of C_{lmax} at slightly higher angles of attack, but to this point they are virtually the same within the error band of the data. The curves then drop off rapidly - the higher the rotation rate, the sharper the drop with respect to angle of attack - and oscillate about a C_l of 1.2 out to 60 degrees. The three lift curves at $\alpha^+ = 0.2$ do not behave in quite the same manner as those at $\alpha^+ = 0.1$. They start out for the first 20 degrees or so with the same slopes as one another but not, as with the lower value, linear. They then deviate somewhat from one another, peaking out at the same value of C_{lmax} of 2.2, but at angles of attack varying from 31 to 41 degrees. There seems to be no specific trend which can be attributed to either rotation rate or flow velocity, since the curve that appears to be in the middle is actually that for the lowest pitch rate. At these high pitch rates this minor anomaly could be attributed to experimental error. The conclusion remains, however, that the non-dimensional pitch rate parameter, α^+, is at this point, the major determining factor for the shape and magnitude of the lift curve. Thus, since curves of constant α^+ are nearly similar, examing the effects of changing α^+ is closely akin to analyzing the effects of changing the pitch rate at constant Reynolds number as in Fig. 3. One can see from there and from Figs. 7 and 8 that increasing α^+ results in increases in $dC_l/d\alpha$, C_{lmax}, and α at C_{lmax}. In addition, lower values of α^+ result in more abrupt decreases in C_l occurring more rapidly after having reached C_{lmax}.

B.   Pressure Coefficient vs x/c

The Appendix contains Figs. A.1 (a), (b), (c), (d) through A.9 (a), (b), (c), (d). The numbers 1-9 correspond to each of the cases shown in Table 1 starting with

$U_\infty = 20\,ft/sec$, $\dot{\alpha} = 230\,deg/sec$, $\alpha^+ = 0.1$, following left to right and ending with $U_\infty = 80\,ft/sec$, $\dot{\alpha} = 920\,deg/sec$, $\alpha^+ = 0.1$. The (a) - (d) discriminants refer to angles of attack of $15°$, $30°$, $45°$, and $60°$ respectively.

Walker et. al. (Ref. 14) presented qualitative data using a smoke-wire flow visualization technique and near-surface single element hot-film velocity magnitude measurements for two cases essentially the same as two of the cases examined herein: $\alpha^+ = 0.2$ and 0.6. In these experiments they observed strong vortices forming above the suction surface of the airfoil due to the shear layer interaction between the freestream and the leading edge separation bubble, formed as the airfoil pitches up and to the added rotational energy imparted to the flow. They were able to correlate the movements of these vortices with velocity magnitude peaks measured with the hot-film sensors. Figs. A.2 and A.4 show the corresponding surface pressure measurement experiments of these two cases; the upper surface pressure peaks are in good agreement with the spatial positions of the vortices.

Fig. A.1 shows the lowest pitch rate examined corresponding to an α^+ of 0.1. Except for the fact that the NACA 0015 airfoil would be stalled at 15 degrees in steady flow, (a) shows a rather ordinary C_p plot for high angles of attack, with the exception of the first 20% of the upper surface. Here one can observe a pressure peak at the 16% chord point indicating the presence of the leading edge vortex. Also, there is no high suction peak very near the leading edge that is present in steady flow. This is true for all of the other cases studied with the exception of the lowest ($\alpha^+ = 0.05$) case. This could, in part, be due to the first sensor location but is more likely due to the interaction of the leading edge vortex reverse flow in the vicinity of the leading edge and the freestream flow producing locally reduced flow velocities. In (b) we can see that the vortex is still producing a great deal of lift and has traversed to a point slightly aft of mid-chord. In (c)

we can now tell that the vortex has separated from the airfoil causing it to stall.

Increasing $a+$ to a value of *0.2*, Fig. A.2 (a) shows characteristics similar to A.1 (a) but higher in value; and then (b) shows a very high pressure peak of almost *-6.0* at *24%* chord indicating the presence of a stronger vortex than previously observed. By the time the airfoil reaches *45°* in (c), the vortex has moved past mid-chord and off the airfoil, substantially reducing lift. At *60°*, the airfoil is completely stalled. Also, an interesting pressure anomaly has entered the picture.

From *8%* to *56%* chord at an angle of attack of *45°*, the lower surface pressure coefficient is slightly greater than one. This could be attributed to experimental error except for two elements: 1) Francis, et. al. (Ref. 11) noticed this sort of phenomenon in their experiments and stated that it should be investigated further; 2) in these sets of experiments, this phenomenon is observed to become more pronounced at higher angles of attack and at higher values of $a+$. It appears to occur at $a+$ levels of *0.2* or greater, where a great deal of rotational energy relative to the freestream is injected into the flow producing large flow curvatures. King (Ref. 19) has pointed out that a *V/r* term from Crocco's theorem as presented in Liepmann and Roshkow (Ref. 20) may be the culprit by increasing the local stagnation pressure.

For the case of $a+ = 0.4$, Fig. A.3 (a) indicates a very high value of C_p over the entire airfoil similar in nature for the previous case but greater in magnitude. At an angle of attack of *30°*, (b) shows a very large peak in C_p of greater than *-9.0* at the *10%* chord point. By the time the airfoil has reached an angle of attack of 45° in (c), the vortex has moved downstream to the *34%* chord point and away from the airfoil. At *60°*, shown in (d), the vortex has moved further downstream but is still exhibiting a great deal of influence on the flowfield around the airfoil.

Fig. A.4 depicts pressure coefficients for the last of the four cases at $U_\infty = $ *20 ft/sec.*

This is the case of the highest $\alpha+$ examined. At $\alpha+ = 0.6$ the airfoil is pitching up at a rate of *1380 deg/sec.* At *15°* in (a), C_p curves look about the same as before except a bit higher. In (b), the vortex hasn't really formed yet, but the pressure peak at *6%* chord is at *-9.8* and the flow is still attached over the entire airfoil. In addition, the maximum lower surface pressure coefficient has reached *1.5.* By *45°* the vortex has fully formed, producing a pressure peak greater than *-14.0* at the *14%* chord point. These conditions have also resulted in a maximum lower surface C_p of *2.0* at *47%* chord. As the airfoil reaches *60°* in (d), the vortex has moved to *24%* chord. As the airfoil reaches *60°* in (d), the vortex has moved to *24%* chord and away from the surface resulting in a reduced C_p of *-9.0.*

Figs. A.5 and A.6 show pressure coefficients for two pitch rates at $U_\infty = $ *40 ft/sec* corresponding to non-dimensional pitch rates of *0.1* and *0.2* respectively. They are remarkably similar to Figs. A.1 and A.2 with only minor differences in peak values and locations.

The only data taken at *60 ft/sec* are for $\alpha+ = 0.2$ with a corresponding pitch rate of *1380 deg/sec* shown in Fig. A.7. Again, as with Fig. A.6, the pressure coefficient data is very similar to that of Fig. A.2 - the only exception being that of A.7 (c), where a relatively high peak is seen at *34%* chord.

Two final sets of experimental data were taken at $U_\infty = $ *80 ft/sec.* These are shown in Figs. A.8 and A.9 for $\alpha+$ values of *0.05* and *0.1* respectively. In A.8 (a) we see C_p curves much like those of unstalled high angles of attack for this airfoil. At *30°* it is apparent that the airfoil has stalled completely, indicating that the leading edge vortex has either not formed or does not have the requisite strength to produce the strong reverse flow velocities observed previously.

Figs. A.9 (a), (c), and (d) look very much like their counterparts in Figs. A.2 and A.5.

A.9 (b), however, is somewhat different. Whereas the first two cases where $a^+ = 0.1$ at an angle of attack of 30° produced suction surface pressure coefficients of -1.5 to -1.8 near the leading edge, increasing to -3.5 at 47% to 53% chord, and dropping to -0.5 at 85% chord, this one starts at -3.0 near the leading edge, peaks at -4.0 at 34% chord, and falls rapidly to -0.5 at 65% chord. While this will produce almost the same lift coefficients, the indication in this case is that the leading edge vortex develops somewhat more rapidly and is somewhat stronger than in the previous $a^+ = 0.1$ cases. Additionally, a greater portion of the aft section of the airfoil is separated.

IV. Conclusions

The experimental pressure measurements presented herein have shown relationships between the unsteady lifting forces on a pitching airfoil and pitch rate, Reynolds number, and non-dimensional pitch rate, a^+. The current investigations were limited to the effects of these parameters on pressure and lift coefficients. With regard to lift coefficients it was seen that, for constant Reynolds number (or flow velocity), increasing pitch rate (or non-dimensional pitch rate) increased C_{lmax}, dC_l/da up to C_{lmax}, and in general, the angle of attack which C_{lmax} occurs. These effects were more dramatic at lower Reynolds numbers. Increasing Reynolds number while holding pitch rate constant had the opposite effect. The effect of holding the non-dimensional pitch rate constant while allowing pitch rate and Reynolds number (flow velocity) to vary is of special interest. For both cases studied, $a^+ = 0.1$ and 0.2, the C_l vs a curves were very similar at constant a^+ - only the angle of attack for C_{lmax} showed inconsistencies at the higher value.

Examination of the non-integrated parameters or pressure coefficients, proved more enlightening. Not only did the C_p vs x/c curves show the same overall effects as the C_l vs a curves did, but they showed the same effects at discrete points on the airfoil.

41

Pressure coefficients at given angles of attack for constant $\alpha+$ values showed the same correlation as the lift coefficients. In addition, the movement of the "dynamic stall" vortices and their effects on the airfoil under different conditions could be determined.

References

1. McCroskey, W.J., "Unsteady Airfoils," Annual Review of Fluid Mechanics, pp 285-311, 1982.

2. Herbst, W.B., "Supermaneuverability," Joint Automatic Control Conference, Univ. of VA, 17-19 Jun 1981; see also Workshop on Unsteady Separated Flow, USAF Academy, 10-11 Aug 1983, published by the Univ. of CO Dept of Aero. Engr. Sci.

3. McCroskey, W.J., and Philippe, J.J., "Unsteady Viscous Flow on Oscillating Airfoils," AIAA J., Vol. 13, No. 1, pp 71-79, Jan 1975.

4. McAlister, K.W., and Carr, L.W., "Water Tunnel Visualization of Dynamic Stall," J. Fluids Engr., Vol. 101, pp376-380, Sep 1978.

5. Martin, J.M, Empey, R.W., McCroskey, W.J., and Caradonne, F.X., "An Experimental Analysis of Dynamic Stall on an Oscillating Airfoil," J. Am. Hel. Soc., Vol. 19, No. 1, pp 26-32, Jan 1973.

6. Robinson, M.C., and Luttges, M.W., "Unsteady Flow Separation and Attachment Induced by Pitching Airfoils," AIAA Paper 83-0131, Jan 1983.

7. Robinson, M.C., and Luttges, M.W., "Unsteady Separated Flow: Forced and Common Vorticity About Oscillating Airfoils," Workshop on Unsteady Separated Flows, pp 117-126, USAF Academy, 10-11 Aug 1983, published by the Univ. of CO Dept. of Aero. Engr. Sci.

8. Carr, L.W., McAlister, K.W., and McCroskey, W.J., "Analysis of the Development of

Dynamic Stall Based on Oscillating Airfoil Experiments," NASA TN D-8382, Jan 1977.

9. Harper, P.W., and Flanigan, R.E., "The Effect of Rate Change of Angle of Attack on the Maximum Lift of a Small Model," NACA TN 2061, 1950.

10. Ham, N.D., and Garelick, M.S., "Dynamic Stall Considerations in Helicopter Rotors," J. Am. Hel. Soc., pp 40-50, Apr 1968.

11. Francis, M.S., Keesee, J.E., and Retelle, J.P., "An Investigation of Airfoil Dynamic Stall with Large Amplitude Motion," FJSRL-TR-83-0010, Oct 1983.

12. Deekins, A.C., and Kuebler, W.R., "A Smoke Tunnel Investigation of Dynamic Separating," Aeronautics Digest, USAFA-TR-79-1, pp 2-16. Feb 1979.

13. Daley, D.C., "The Experimental Investigation of Dynamic Stall," Thesis, AFIT/GAE/AA/820-6, Air Force Inst. Of Tech., WPAFB, OH, 1983.

14. Walker, J.M., Helin, H.E., and Strickland, J.H., "An Experimental Investigation of an Airfoil Undergoing Large Amplitude Pitching Motions," AIAA. Paper 85-0039, The Aerospace Sciences Conference, Reno, NV, Jan 1985.

15. Helin, H.E., and Walker, J.M., "Interrelated Effects of Pitch Rate and Pivot Point on Airfoil Dynamic Stall," AIAA Paper 85-0130, The Aerospace Sciences Conference, Reno, NM, Jan 1985.

16. Francis, M.S., Keesee, J.E., and Retelle, J.P., "A Two-Degree-of-Freedom Oscillator for Unsteady Aerodynamics Applications," FJSRL-TR-81-0007, Jul 1981.

17. Gormont, R.E., "A Mathematical Model of Unsteady Aerodynamics and Radial Flow for Application to Helicopter Rotors," U.S. Army AMRDL Technical Report 72-67, 1973.

18. Strickland, J.H., and Graham, G.M., "A Dynamic Stall Inception Correlation for Airfoils Undergoing Constant Pitch Rate Motions," Technical Note submitted to AIAA for publication in AIAA J., Sep 1984.

19. King, P., private conversation, Jan 1985.

20. Liepmann, H.W., and Roshko, A., Elements of Gas Dynamics, Galcit Aeronautical

Series, John Wiley and Sons, Inc., New York, 1957.

APPENDIX
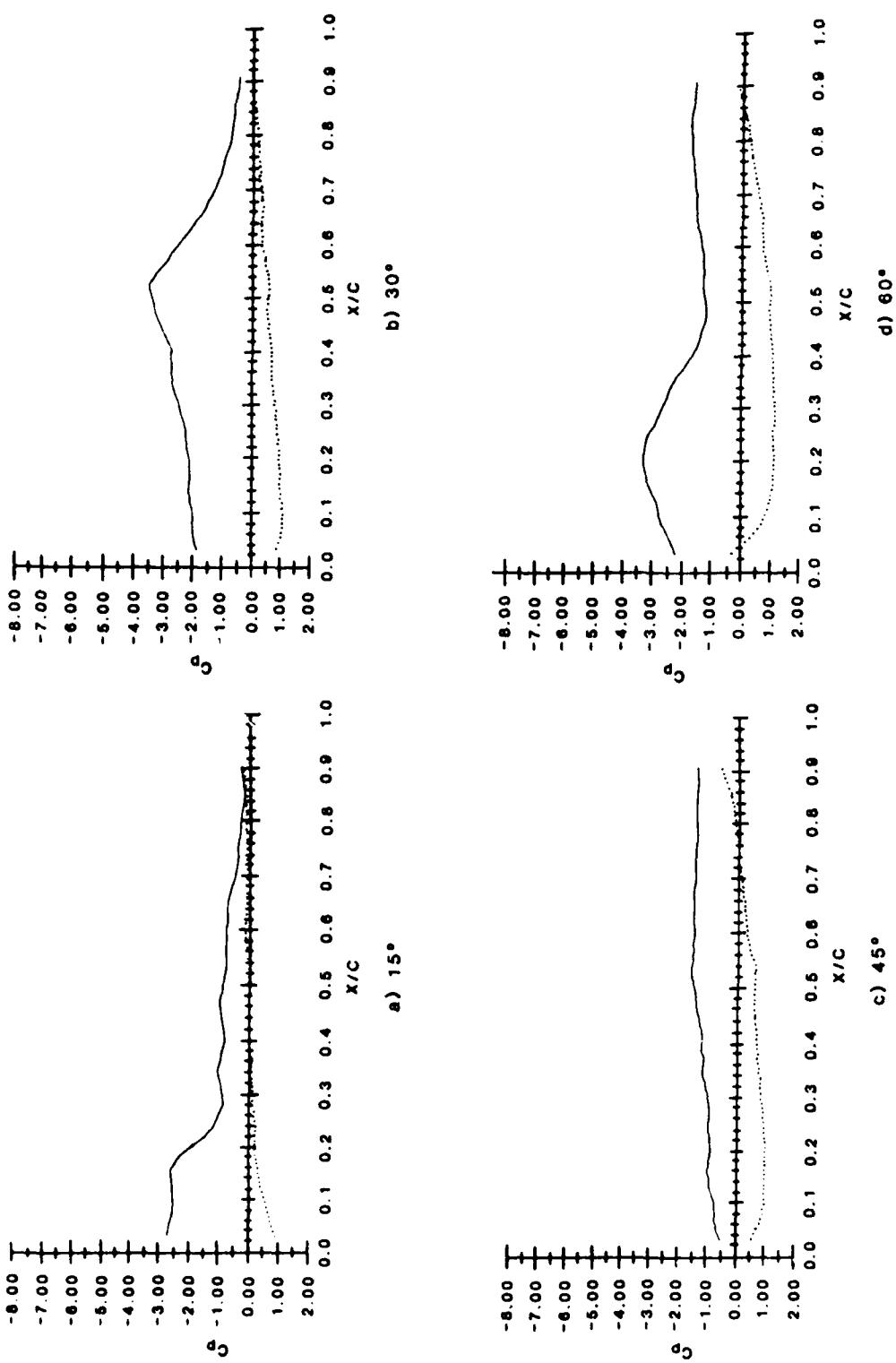
Figure A.1 $\alpha^+ = 0.1$, $\dot{\alpha} = 230^\circ/s$, $U_\infty = 20$ f/s
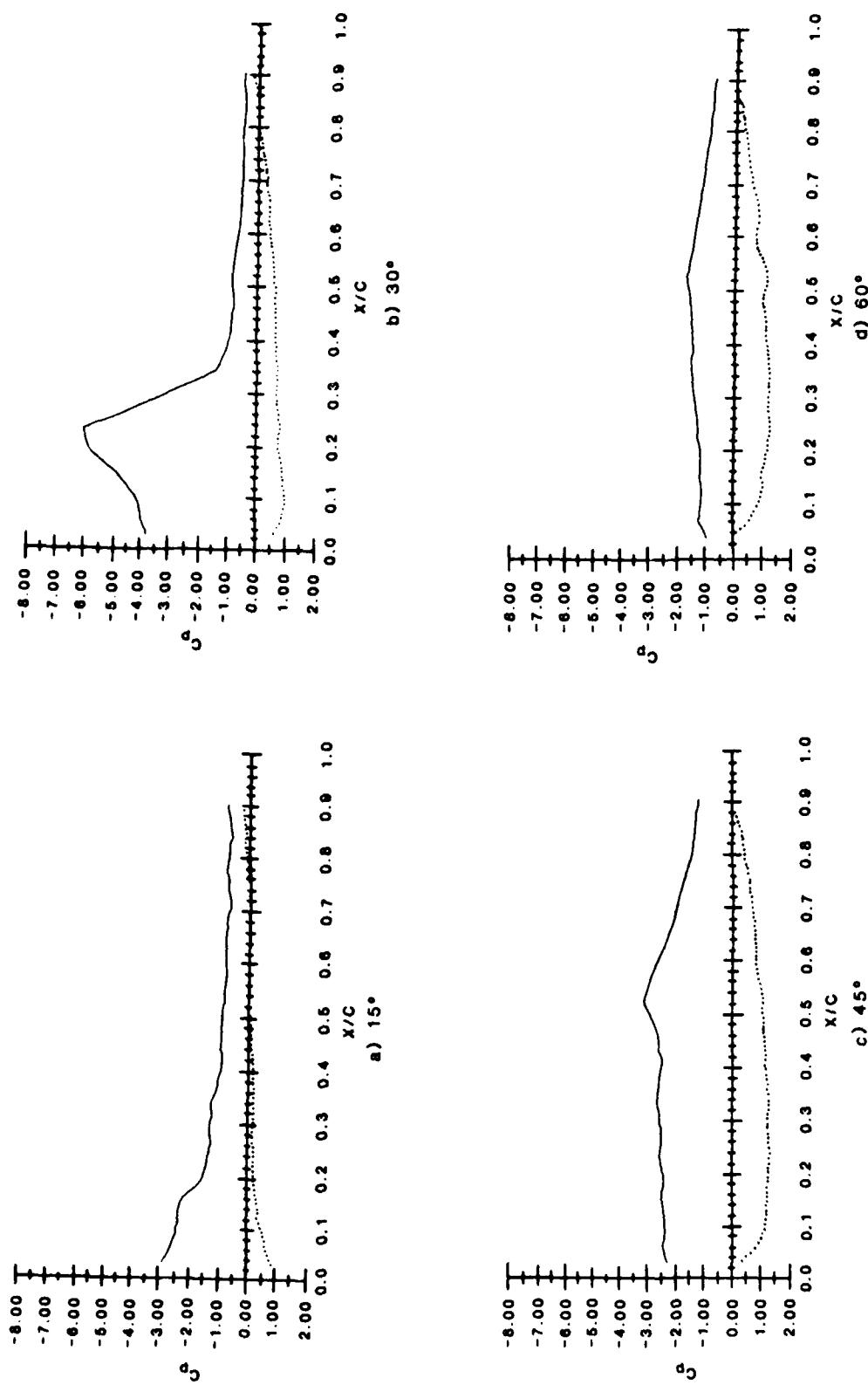
Figure A.2 $\alpha+ = 0.2$, $\dot{\alpha} = 460°/s$, $U_\infty = 20f/s$
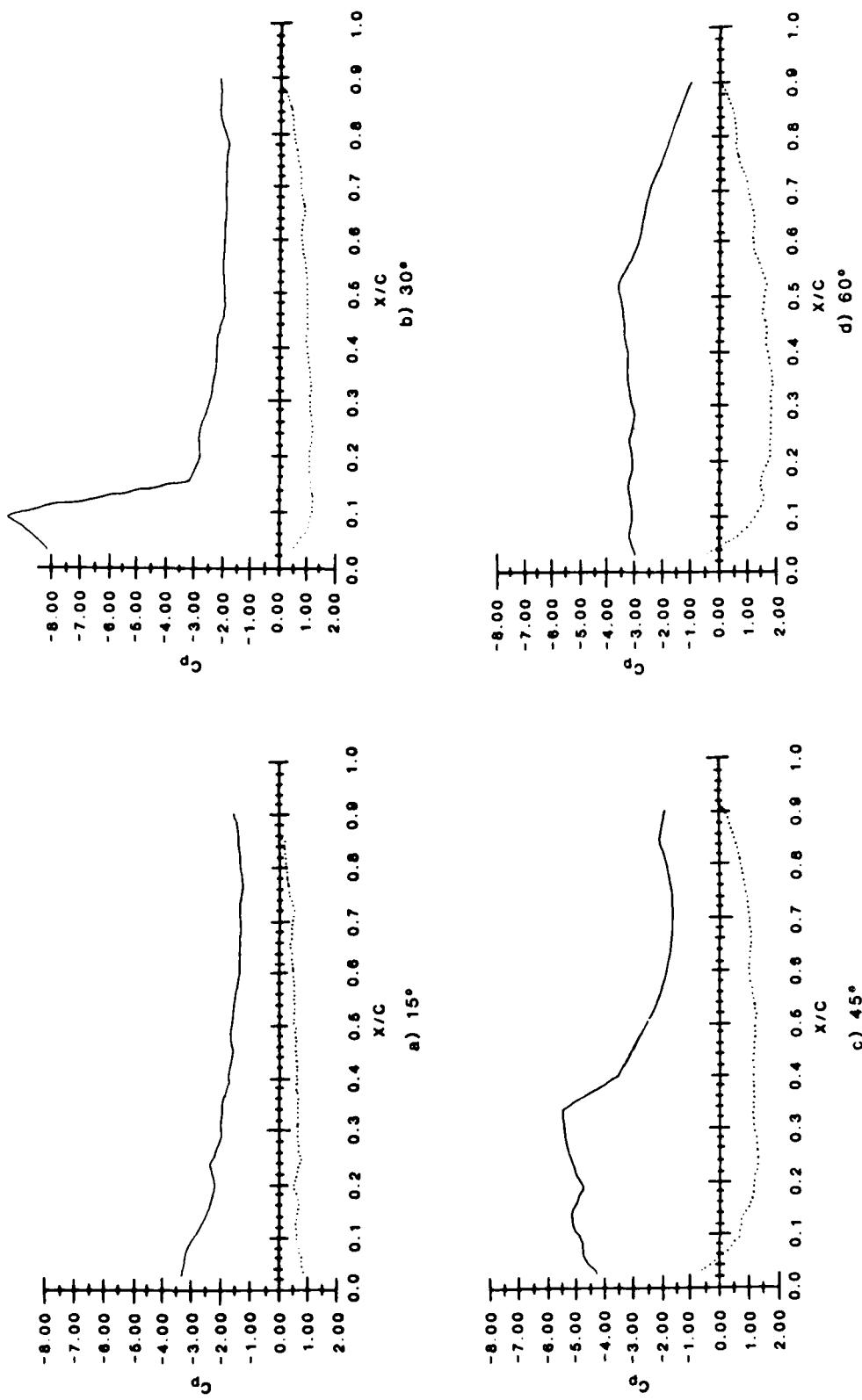
Figure A.3 $\alpha + = 0.4, \dot{\alpha} = 920^\circ/s, U_\infty = 20$ f/s
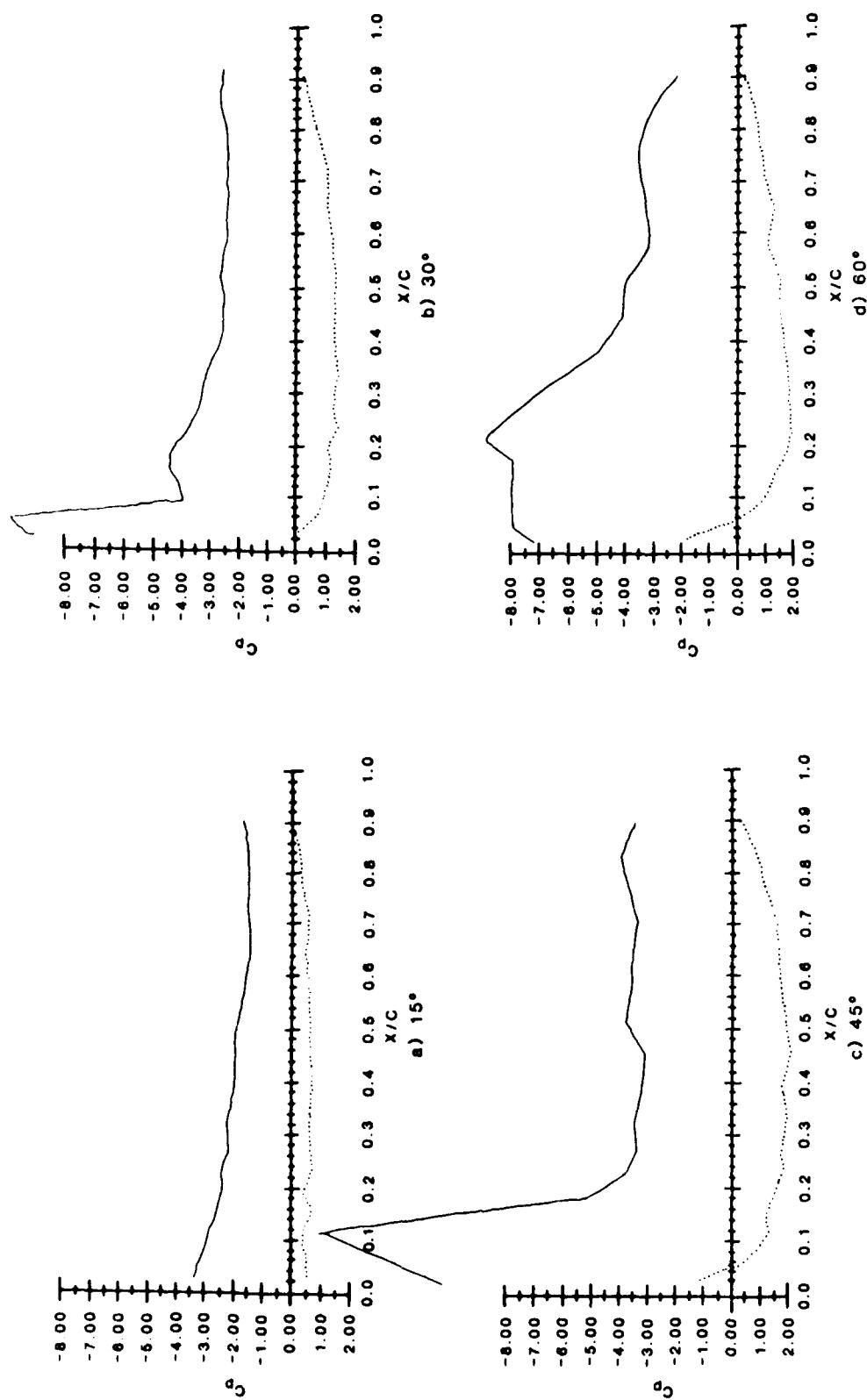
Figure A.4 $\alpha^+ = 0.6$, $\dot{\alpha} = 1380°/s$, $U_\infty = 20f/s$
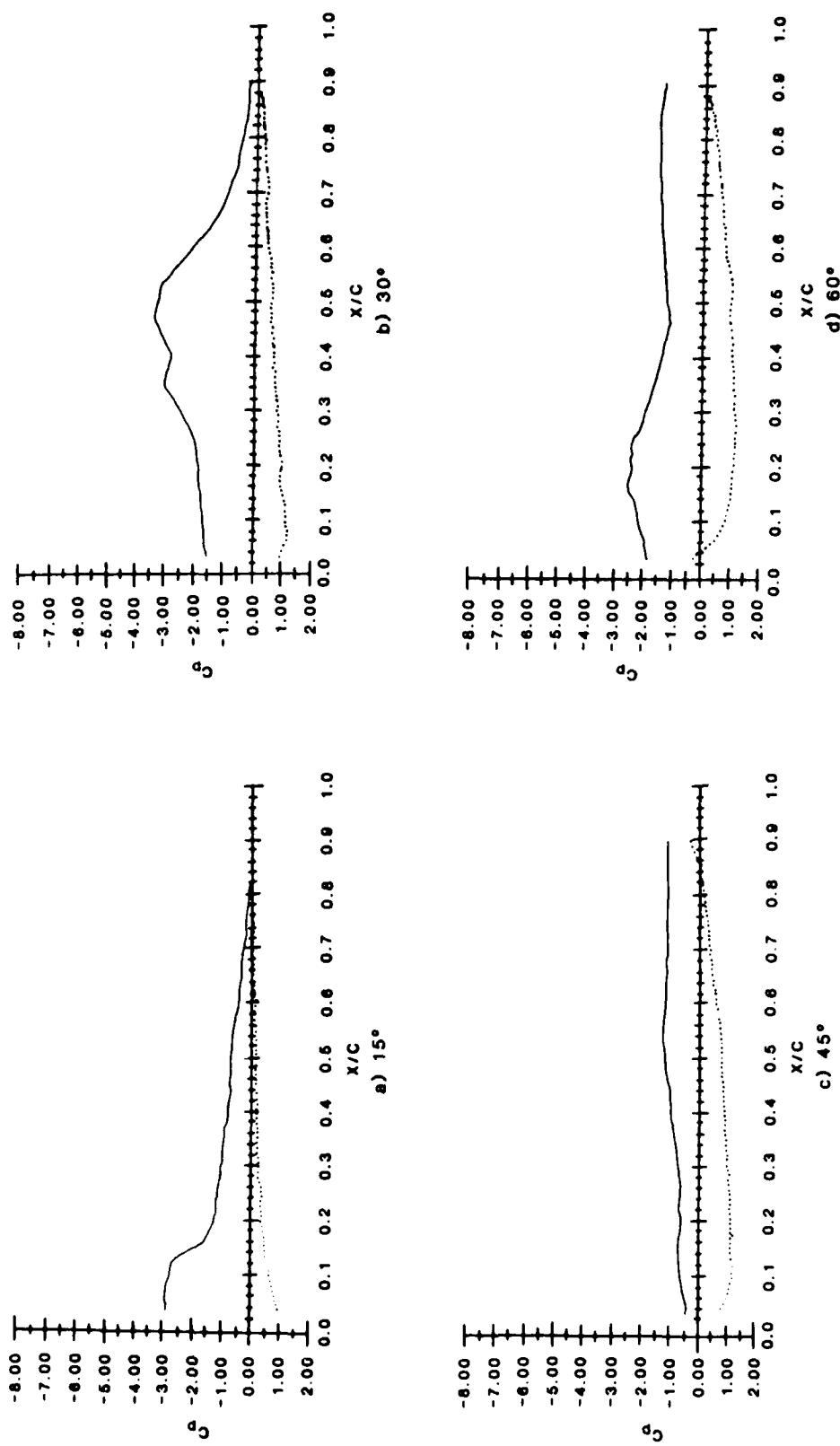
Figure A.5 $\alpha^+ = 0.1$, $\dot{\alpha} = 460°/s$, $U_\infty = 40 \, f/s$
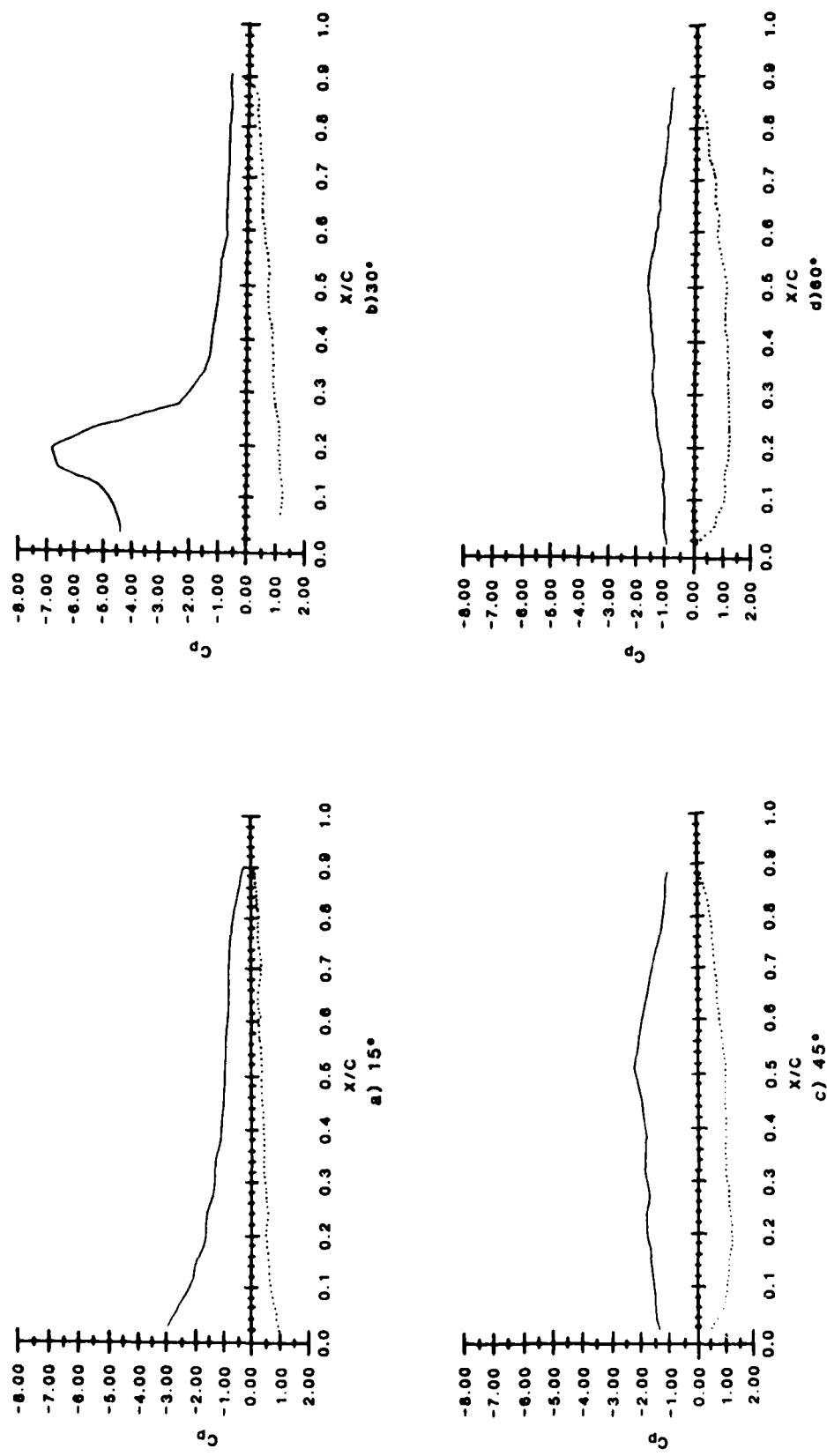
Figure A.6 $\alpha^+ = 0.2$, $\dot{\alpha} = 920°/s$, $U_\infty = 40f/s$
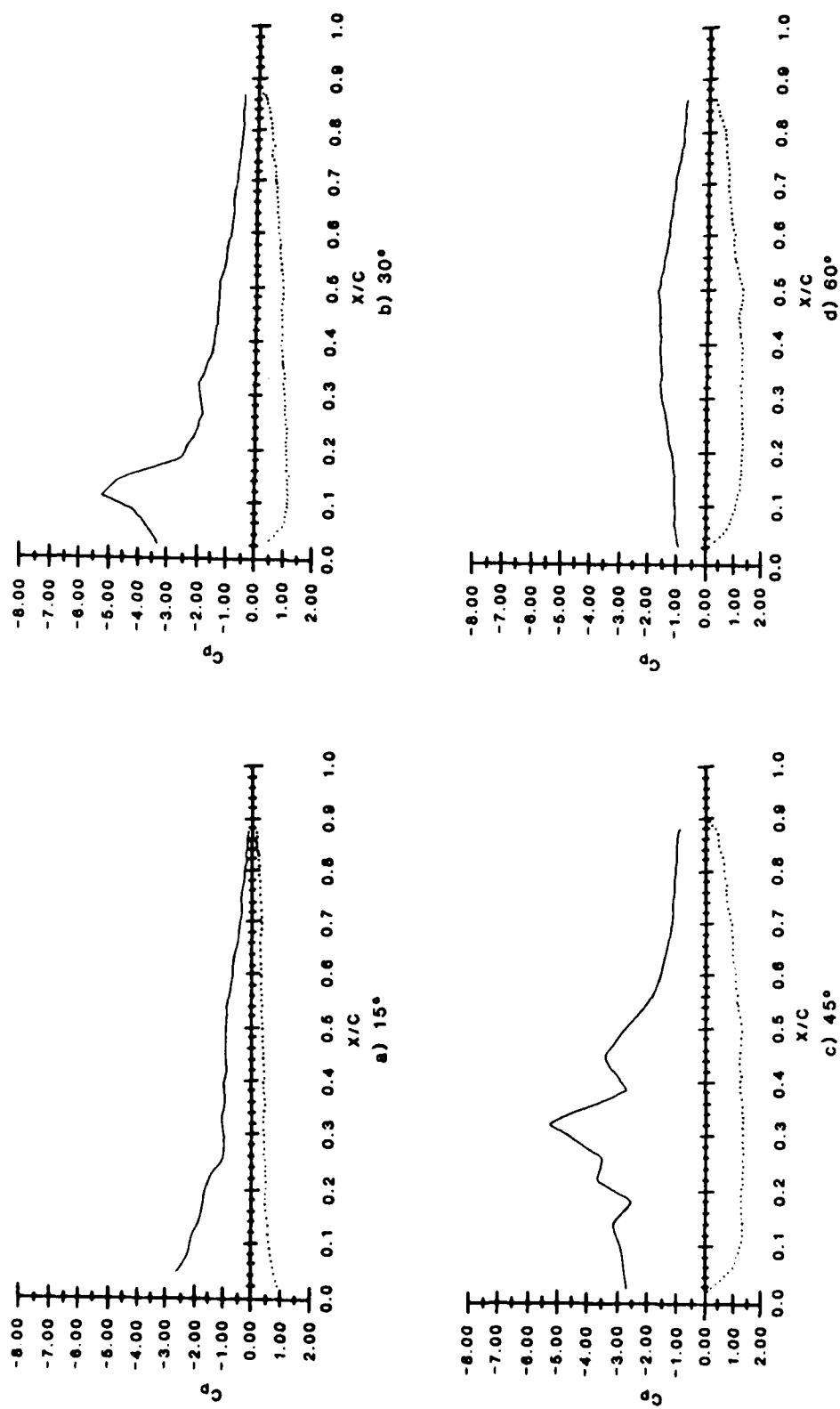
Figure A.7 $a^+ = 0.2, \dot{a} = 1380°/s, U_\infty = 60$ f/s
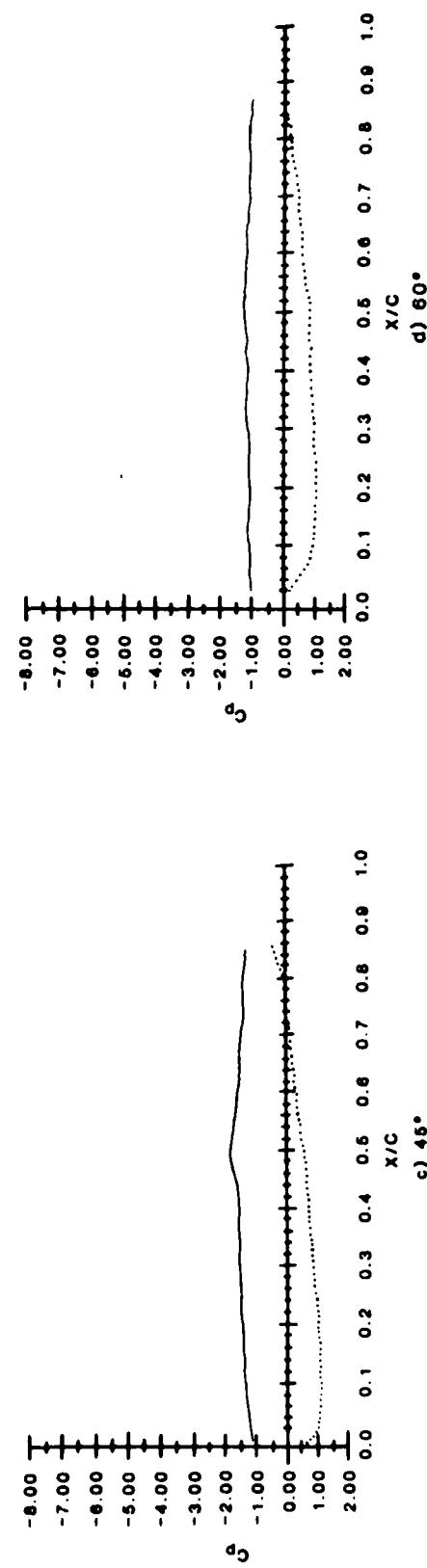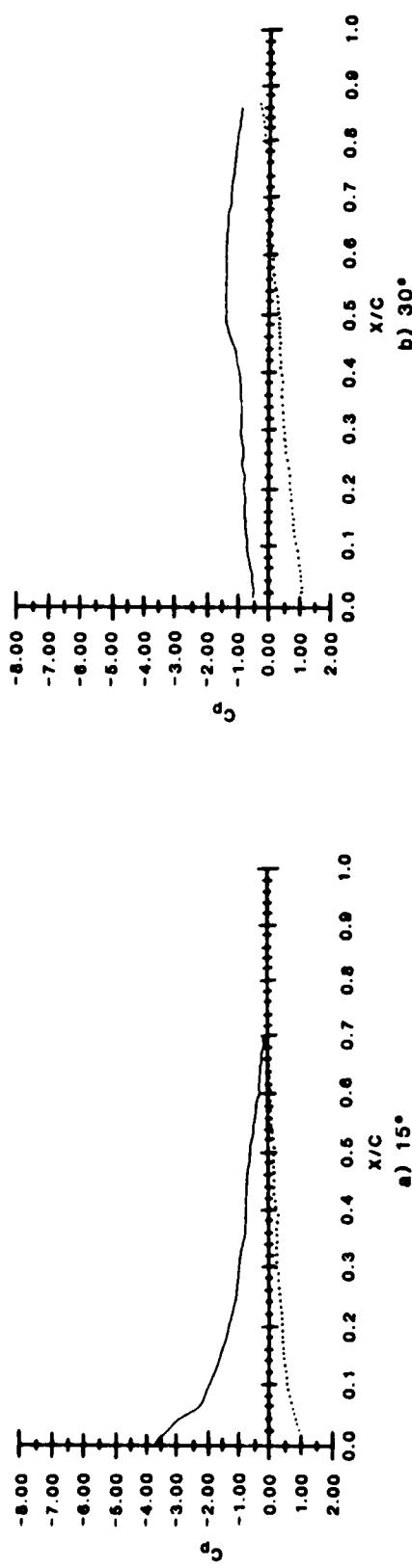
Figure A.8 $a^+ = 0.05$, $\dot{a} = 460°/s$, $U_\infty = 80f/s$

Figure A.9 $\alpha + = 0.1$, $\dot{\alpha} = 920°/s$, $U_\infty = 80f/s$

54
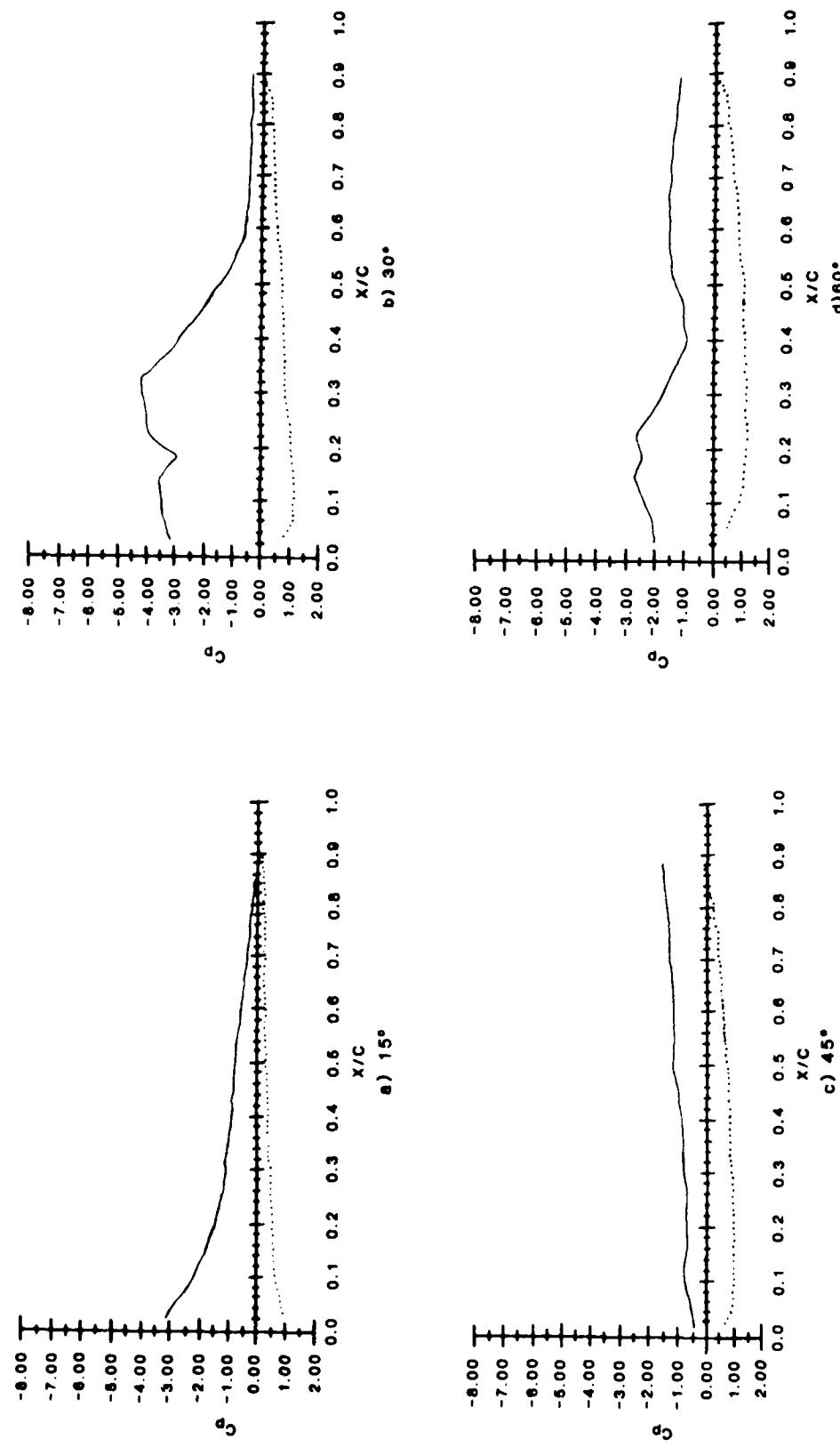
Undergraduate Airbreathing Propulsion At The US Air Force Academy

Jack D. Mattingly* and William H. Heiser**

Abstract

This paper summarizes the status of the teaching of airbreathing propulsion to the undergraduate students at the U.S. Air Force Academy. This is one of the most active and productive propulsion curricula in the country. The emphasis of this article is on course philosophy and content in general, and on the goals and experiences of the flagship course on propulsion design in particular.

I. Introduction

A very active curriculum in airbreathing propulsion exists in the Department of Aeronautics of the U.S. Air Force Academy, for a number of mutually supportive reasons. To begin with, many cadets attend the Academy in order to become pilots; therefore, they have a natural curiosity about and a vital interest in how jet engines work. Furthermore, the cadets realize that such knowledge will be necessary because their careers are likely to include one or more interesting and important assignments in laboratories, procurement offices, maintenance, ground and flight test, or as staffs of the Commands and Pentagon. Finally, unusually heavy support for the curriculum is available in the form of a faculty rich in experience in the development and operation of aircraft engines, generous supplies of computer time and codes, and immediate access to excellent laboratory facilities.

In fact, the Aeronautics Laboratory may be the only place in the country with enough financial and logistic support to allow undergraduate students to routinely experiment

---

* Lt. Col., USAF, Associate Professor, Dept. of Aeronautics, USAF Academy, CO.
** Formerly Professor, The Univ. of Tennessee Space Institute, Tullahoma, TN; Distinguished Visiting Professor, Dept. of Aeronautics, USAF Academy, CO. Currently Vice-Pres./Director, Propulsion Research Inst., Aerojet General, Sacramento, CA.

with real jet engines. The laboratory has four engine test cells (see Table 1). Three are dedicated to the testing of jet engines and one is dedicated to solid propellant rocket thrust tests and internal combustion engine testing.

Table 1 Aeronautics Laboratory Propulsion Equipment

Test Cell #	Description
1	One J85 turbojet engine -2800 lb thrust, non- augmented
2,3	Two J69 turbojet engines -1000 lb thrust (one is planned to be replaced by an F109 turbofan engine - 1300 lb thrust)
4	5" diameter solid propellant rocket motor (500 lb thrust, 3 sec burn time, $C^* \approx 5000$ ft/sec)

All cadets graduating from the Academy (approximately 1,000/year) perform a static thrust test with the J69 turbojet engines as part of the "Engineering Thermodynamics" course (a required course for all graduates) taught by the Department of Aeronautics. Since the students are interested in and curious about the operation of airbreathing engines and rocket nozzles, this course demonstrates the application of engineering thermodynamics by analyzing these machines. The static thrust test provides the opportunity to compare analytical and experimental results.

The result of these forces is a successful aeronautical engineering program which educates approximately 80 new cadets each year, and was the breeding ground (in 1976) for the famous "Oates Notes" (Ref. 1), which have become the bestselling AIAA Education Series Book, The Aerothermodynamics of Gas Turbine and Rocket Propulsion , by Gordon C. Oates.

II. The Curriculum

The aeronautical engineering major is currently composed of thirty-three semester hours of major courses in addition to the 111 semester hours contained in the Academy's Core Curriculum. Because of the limited number of courses in the major, topics that typically would be taught in separate courses are combined and split between courses to

provide the required coverage. For example, gas dynamics is incorporated into both the Propulsion I course (one-dimensional flow) and the Aerodynamics II course (two-dimensional flow). The curriculum (Table 2) provides the opportunity for student choice of design course (6 semester hour course) and one Aero option. Thus the student can emphasize a specific area of interest, such as flight mechanics, propulsion, aerodynamics, or structures.

Table 2 Aeronautical Engineering Major

```
· 111   Semester hours of core courses
·  33   Semester hours of major courses


    ·  Junior Year
       -  Flight Mechanics I
       -  Propulsion I
       -  Aerodynamics I
       -  Aerodynamic Structures
       -  Analytical & Numerical Methods
          in Aeronautics

    ·  Senior Year
       -  Aeronautical Laboratory
       -  Aerothermodynamics
       -  Aerodynamics II
       -  Design Option -  Aircraft Design or
                           Propulsion Design
       -  Aero Option   -  Flight Mechanics II
                           Propulsion II
                           Flight Test Techniques
                           Special Topics
                           Independent Study
```

The "propulsion track" is the equivalent of an undergraduate minor in airbreathing propulsion. It consists of three courses, usually taken in sequence, which carry the student from the fundamental principles through to the complete design of an engine which can accomplish a very specific mission. The three courses will now be described in their natural order.

1. Propulsion I

    This introductory course is required in order to obtain an Aeronautics degree at the Academy. It equates to a three unit course in the semester system, and includes the aforementioned 80 students annually. The emphasis of the course is upon the aerodynamic and thermodynamic behavior of the one-dimensional flow of calorically perfect gases. The central feature of the course is the development of methods to relate the overall performance to internal design parameters of rocket and gas turbine engines, in the manner of Oates (Ref. 1). This feature receives special emphasis because every student participates in one rocket firing and one gas turbine engine run where experimental data is systematically compared with predictions. The influence of the propulsion system and the proper engine cycle on aircraft performance are learned through a design project. For the repetitive calculations required in the design project, students use computer codes based on the on-design and off-design cycle analysis presented in class.

    Further insight into the content and flow of this course can be obtained by looking at the formal table of contents below.

- One Dimensional Flows
  - Review of fundamental laws
  - Normal and oblique shock waves
  - Duct flow with heating, friction, and area change
- Rocket Propulsion
  - Performance definition and prediction
  - Nozzle theory and design
  - Rocket motor laboratory test
- Aircraft Propulsion
  - General concepts (energy chain and installed vs. uninstalled thrust)
  - Design point cycle analysis:
    - ideal ramjet
    - ideal turbojet
    - ideal afterburning turbojet
    - ideal turbofan
    - real turbojet
    - real afterburning turbojet
    - real turbofan

                    sensitivity analysis
                    optimum performance
        -    Off-design cycle analysis:
                    real turbojet
                    real turbofan
        -    Components:
                    inlets
                    compressors
                    burners
                    turbines
                    afterburners
                    nozzles
        -    Turbine engine laboratory test
        -    Cycle design project

2.   Propulsion II

    This course also equates to three units in the semester system, and includes about

20 students annually. The emphasis is upon qualitative and quantitative aspects of the

design of the major components of turbine engines.   For example, methods are

developed which enable the design of compressor and turbine stages and inlet

configurations, as well as the calculation of the products of combustion reactions. Also

included is the analysis of more advanced jet engine cycles, and a final project which tests

the understanding of several of the course topics at once.

    Although this is generally considered as preparation for the design course which

follows, it need not necessarily be taken for that purpose. Some students terminate with

this course, a few others take it simultaneously with the design course, and others

occasionally go on to the design course without it. Further appreciation of the scope

should be made possible by the formal table of contents below.

    ·   Compressor Design
        -    Cascade aerodynamics
        -    Stage selection
        -    Radial equilibrium
        -    Multi-staging
        -    Reduced compressor map
        -    Post-stall behavior
    ·   Turbine Design
        -    Cascade aerodynamics
        -    Work relationships

- Structural analysis
- Component Matching and Sizing
- Combustion Chemistry
  - Mixtures of perfect gases
  - Concepts (heat of reaction, equilibrium, law of mass action)
  - Chamber condition calculations
  - Equilibrium and frozen nozzle flows
  - Chemical kinetics
- Stationary Components
  - Inlets
  - Burners
  - Mixers
  - Afterburners
  - Nozzles
- Advanced Cycles
  - Turbofan with mixing and afterburning (on- and off-design)
  - Thrust augmentation devices
- Component Design Project

3. Propulsion Design

This is both the centerpiece and the culmination of the "propulsion track." It is a double-unit course, equaling two three-unit courses in the semester system, and including about 20 students annually. In contrast to the two preceding courses, which strongly emphasize basic concepts and specific analytical tools, this course contains many features which are intended to reproduce the design experience via the design of an engine.

There is no absolute roadmap for the design of a gas turbine engine. The steps involved depend, for example, on the experience of the company and the people involved, as well as on the nature of the project. A revolutionary new engine will require more analysis and iteration than the modification of an existing powerplant. Nevertheless, there are generalized representations of the design process which are informative and useful. One of these, which depicts the entire development process, is shown in Fig. 1 which is taken from Gas Turbine Theory by Cohen, et al (Ref. 2). The portion of Fig. 1 enclosed by the dashed line is of paramount importance here because that is the territory covered by this course. Although the boundary can be somewhat
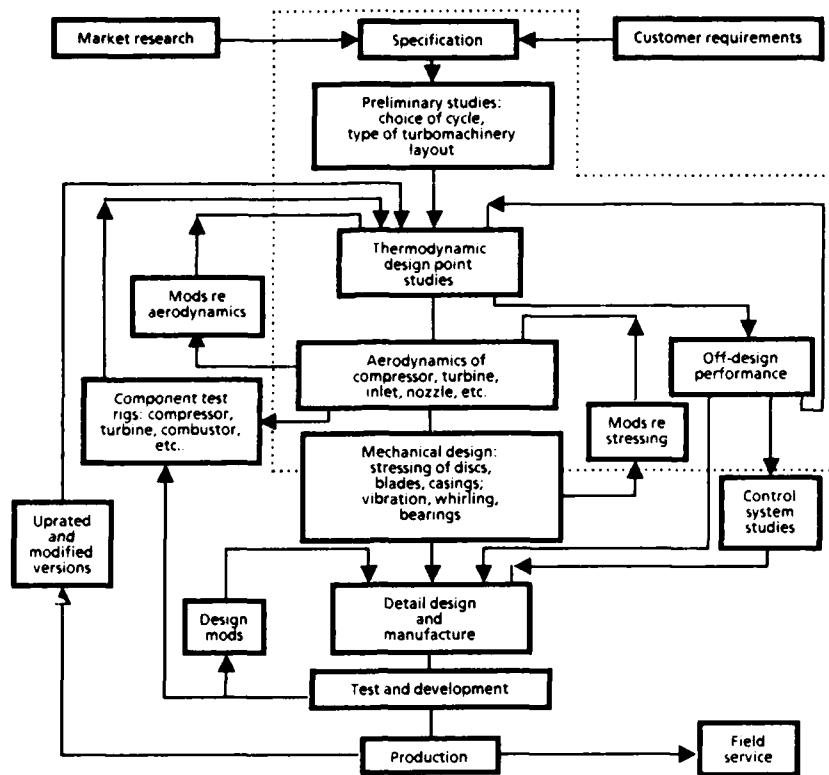
Figure 1. Gas Turbine Engine Design System

altered, for example by including control system studies, it can never encompass the hardware phases, such as manufacturing and testing.

We would like to make clear what we believe is special about the design process, for that is what this course attempts to make happen. Every designer has a mental description of what designing really is, so our version is not likely to be exhaustive. Nevertheless, the list below contains critical elements with which few would disagree.

· The design process is both started by and constrained by an identified need.

· Although many legitimate solutions exist, none can be identified as unique or optimum. The final selection always involves judgment and compromise.

· In the case of systems design, such as aircraft and engines, too many legitimate solutions exist. Systematic methods must be found to home in on the best.

- The process is inherently iterative, often requiring the return to an earlier step when prior assumptions lead to a dead end.

- Many technical specialties are interwoven. For example, gas turbine engine design involves at least thermodynamics, aerodynamics, heat transfer, combustion, structures, materials, manufacturing processes, instrumentation, and controls.

- Above all, the design of a complex system requires active participation and disciplined communication by every one involved. Because each part of the system influences all the others, the best solutions can only be discovered (and major problems and conflicts avoided) if the participants share their findings clearly and regularly.

Some of the special features we have found that greatly contribute to the accomplishment of these goals include:

- Basing the design on a contemporary Request for Proposal (RFP) provided by an interested, outside "sponsor", such as the Air Force Flight Dynamics Laboratory (AFFDL) or the Air Force Air Staff. Figure 2 shows the mission of a recent project sponsored by AFFDL.

- Working in concert with an aircraft design course on the same RFP, in which case they play the role of an airplane company. Frequent contact and negotiation between courses helps improve results, while providing a lot of reality.

- Supplying very user friendly computer codes for engine on- and off-design cycle analysis, along with liberal amounts of computer time, so that the students can concentrate on the real objective of finding the "best" solutions.
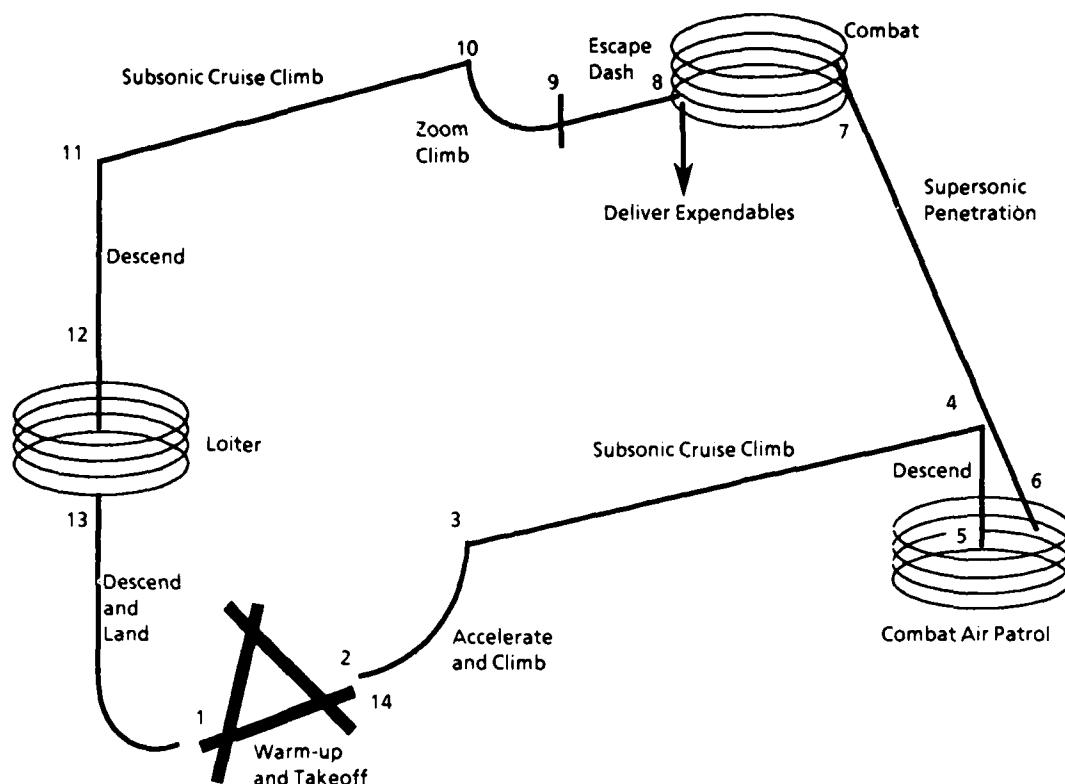
Figure 2. Air-to-Air Fighter Mission Profile

- Requiring individual design of specific components (e.g. fan, burner, turbine, nozzle) along with correct aerothermodynamic, mechanical and geometrical inter-relationships. This emphasizes the need for frequent, disciplined communications, and culminates in a single design drawing of the integrated engine as a proof test.

- Recycling results when necessary to reach the "best" solution.

- Scheduling periodic written and/or verbal reports in order to insure the flow of information, and to sharpen communication skills.

- Rotating leadership roles (e.g. program manager, chief engineer, vice president of engineering) among students in order to familiarize them with the experiences of organizing and managing.

The design process as modified for this course is shown in Fig. 3 and the formal course content which is intended to achieve these goals is as follows:

- Engine/Aircraft System Constraint Analysis
  - Takeoff thrust-to-weight (thrust loading)
  - Takeoff weight-to-wing area (wing loading)
- Engine/Aircraft System Mission Analysis
  - Takeoff thrust
  - Takeoff weight
  - Takeoff wing area
  - Specific excess power (P_s)
- Engine Design Point Analysis
  - Ranges of design parameters
  - Initial performance estimates
- Engine Off-Design Analysis
  - Selection of design parameters
  - Installation penalties
  - Sizing
  - Throttling
  - Final performance analysis
  - Takeoff thrust
  - Takeoff weight
  - Internal flow properties
- Component Design
  - Aerothermodynamic
  - Structural
- Subsystem Design
- Engine Layout
- Reports and Presentations

We have come to recognize two events that are somehow intimately connected to the success of Propulsion Design. First, the emotional rewards are highest when it appears that a successful engine cannot be found at some point during the design cycle. When the barriers (not the rules) are legitimately broken by the usual method of exhaustively searching for innovative solutions, the loose coalition of frustrated students is transformed into a confident team. Moreover, the lesson has real applicability to their prospective careers in engineering. Second, there seems always to be at least one moment at which the entire class makes a mistake of unimaginably large proportions. Examples of this have included area mismatches between components, designing an
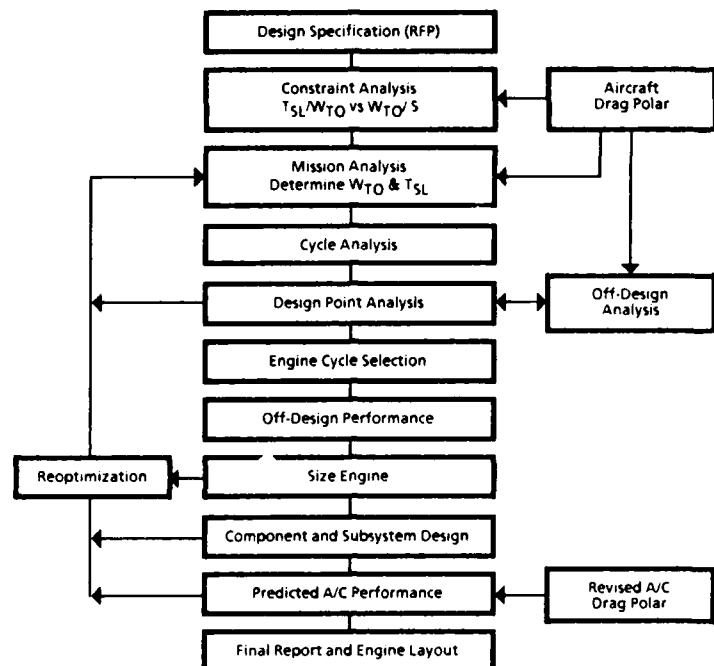
Figure 3. Propulsion Design Course

engine with the airflow intended for two, or the compressor and turbine attached to the same shaft having different rotational speeds. These episodes have a very sobering effect on the students and, after the recriminations dwindle away, result in a far greater appreciation of the vital need for frequent, accurate, and intelligent communication.

Through the entire design process, it is less important that specific milestones be reached according to a preset schedule than that the students achieve comprehension of each successive step, and that they believe in their ownership of the design decisions. This, above all things, makes their experience take life.

III. Texts

The propulsion curriculum has been based on the analytical methods for cycle and component analysis as set down by Gordon C. Oates in "Oates Notes" during 1975-76 while a Distinguished Visiting Professor with the Department of Aeronautics. Starting in 1979, portions of the famous "Red Book" (The Aerothermodynamics of Aircraft Gas Turbine Engines, AFAPL-TR-78-52, July 1978) were incorporated into the Propulsion II and

Propulsion Design courses. The textbooks used in all three courses have evolved over the past decade (see Table 3) and continue today.

Table 3 Textbooks from 1976-85

Propulsion I
- "Oates Notes"
- Elements of Propulsion, edited by Major Jack D. Mattingly*
- The Jet Age, *Forty Years of Jet Aviation*, edited by Boyne and Lopez*
- The Aerothermodynamics of Gas Turbine and Rocket Propulsion, by Gordon C. Oates*

Propulsion II
- "Oates Notes"
- Elements of Propulsion, edited by Major Jack D. Mattingly*
- The Aerothermodynamics of Gas Turbine and Rocket Propulsion, by Gordon C. Oates*
- Aircraft Gas Turbine Engine Technology, by Irwin E. Traeger*
- Red Book ("The Aerothermodynamics of Aircraft Gas Turbine Engines," AFAPL-TR-78-52, July 1978)**

Propulsion Design
- "Oates Notes"
- Elements of Propulsion, edited by Major Jack D. Mattingly*
- The Aerothermodynamics of Gas Turbine and Rocket Propulsion, by Gordon C. Oates*
- Aircraft Gas Turbine Engine Technology, by Irwin E. Traeger*
- Red Book ("The Aerothermodynamics of Aircraft Gas Turbine Engines," AFAPL-TR-78-52, July 1978)**
- Fundamentals of Aircraft Design by Leland M. Nicolai**

*   Current text
** Reference

The cycle analyses of "Oates Notes" were incorporated with fundamental gas dynamics by Major Jack Mattingly in 1982 to produce Elements of Propulsion, the current text of the Propulsion I course. This Academy text is supplemented with readings about the early development of gas turbine engines from The Jet Age, *Forty Years of Jet Aviation*, edited by Boyne and Lopez and published by the National Air and Space Museum. Starting this past spring, the Propulsion I course began use of The Aerothermodynamics of Gas Turbine and Rocket Propulsion, by Gordon C. Oates to supplement the material contained in the other books.

The Propulsion II course is currently using both Oates' The Aerothermodynamics of Gas Turbine and Rocket Propulsion and Aircraft Gas Turbine Engine Technology, by Irwin E. Traeger. The text by Traeger provides excellent material on component and engine construction which goes hand-in-hand with our cut-away displays of J69 and J85 engines.

The Propulsion Design course uses numerous handouts that are supplemented by Elements of Propulsion, The Aerothermodynamics of Aircraft Gas Turbine Engines, and Aircraft Gas Turbine Engine Technology. The methodology of the constraint analysis and the mission analysis used in the Propulsion Design course have their origins in Fundamentals of Aircraft Design by Leland M. Nicolai (Ref. 3).

IV. The Benefits Cascade

We are obviously very enthusiastic about the U.S. Air Force Academy Department of Aeronautics propulsion track, and especially Propulsion Design, and with good reason. Cadets almost invariably rate the latter " the best course they have ever had." The quantitative results have always looked very much like the "real world" solution. In fact, the students often find useful improvements to the RFP and/or inevitable characteristics of the resulting engines before they are generally known elsewhere.

These activities have led to a successful summer Propulsion Workshop at the Academy, which is a blend of basic cycle training, computer-aided cycle selection, and informational briefings on all aspects of USAF involvement with engine research, design, development, acquisition, operation, and maintenance. Finally, another textbook is in the works, which is based upon and will capture the spirit and methodology of Propulsion Design. This textbook is programmed for publication as a part of the AIAA Education Series in 1986 as Aircraft Engine Design.

References

1. Oates, Gordon C., Notes on Rocket and Airbreathing Engines, Vol. I and II, U.S. Air Force Academy, CO, 1976.

2. Cohen, H., G.F.C. Rogers, and H.I.H. Saravanamuttoo, Gas Turbine Theory, John Wiley and Sons, New York, NY, 1972.

3. Nicolai, Leland M., _Fundamentals of Aircraft Design_, METS, Inc., San Jose, CA, 1975.

How To Fairly Account For An Excused Exam

Robert C. Winn*

Abstract

This paper describes a methodical procedure for accurately assigning a course grade to a student who has had one or more exams excused. Simply excluding that exam from the student's average may not be fair to that student or to the other students in the course, depending on the relative difficulty of the excused exam. An equation is presented in order to calculate an imaginary score for the excused exam, a score which is consistent with the student's performance on past exams. Further, a computer program called FAKEGRD , which automates the calculation of the imaginary scores is presented.

I.   Introduction

In the last few years, the workload in the Department of Aeronautics has increased

to the point that specific efforts to reduce it have been considered. One policy change

which was implemented was the elimination of the requirement for make-up exams.

Historically, make-up exams were required for all tests and course quizzes unless

extraordinary circumstances existed. This put a large burden on the course director

because the additional exams were time consuming to prepare, particularly due to the

difficulty in ensuring equivalence between exams. Eliminating make-up exams clearly

had the potential to reduce instructor workload.

However, before excusing a cadet from a graded event, the instructor must answer

a very important question--How does he or she assign a valid course grade? Imbedded in

this question are two other concerns. First, how much testing is enough to determine a

valid grade for any cadet, and second, how should a cadet's grade be determined if an

exam is excused? For the purpose of this paper, I will assume that there is enough

evaluation of each student to allow the excusal of one or two exams. Determining just

how much testing is enough to establish a valid course grade is a complex question and

---

*Major, USAF, Associate Prof. , Dept. of Aeronautics, USAF Academy, CO.

will not be addressed here. In this paper, I will concentrate on the question of how to account for an excused exam in the assignment of a final course grade.

II.   What to Do About an Excused Exam

In the past, when a student was excused from an exam, that score was simply left out of the calculation of the student average. If all exams had identical means and standard deviations, then this method was fine. If, however, the exams varied in difficulty, then some real problems could occur. If a student missed a very difficult exam, his course average would be higher than it should be. The converse was also true.

Table 1
Sample Grades with Excused Exams

	Student A	Student B	Course Average	Course Std Dev	Maximum Possible
Test #1	70	70	70	10	100
Test #2	--	70	60	20	100
Test #3	70	--	80	5	100
AVG.	70.00	70.00	70.00		

The example depicted in Table 1 shows what can happen if missed exams are not accounted for properly. Both students have exactly the same average, but they have not performed equally. Test #2 was a very difficult one with a large standard deviation. Test #3 was very easy with a low standard deviation. Student A did average on Test #1 but well below average (2 standard deviations) on Test #3. Because he didn't take the difficult Test #2, his average is unrealistically high. Student B happened to miss the easy Test #3. As a result, he has the same average as Student A even though he equaled or exceeded the mean on every exam. This example points out the dangers associated with using uncorrected averages when an exam is excused.

If you examine the scores in the above example, you can see some logic that will result in a fairer grade for both students. Student A was a total of 10 points below the

mean on the two exams he took. More accurately, he was 2 standard deviations below the mean for the two exams or an average of 1 standard deviation below the mean per exam. Therefore, the best estimate of what his performance would have been on the exam he missed is 1 standard deviation below the mean on the exam or a score of 40%. Similarly, Student B would be expected to earn a score of 81.25%, 0.25 standard deviations above the mean, on Test #3. By using these imaginary grades in the calculation of the students' averages, Student A ends up with an average of 60% compared to 73.75% for Student B. The effect of including these imaginary scores in a student's average is to increase the weight of the exams he did take. The new averages are a much better indication of student performance in the course.

The above example was a rather drastic one because of the large differences in standard deviations from one exam to another. A more realistic example is taken from Fall 84 Aero 371 as shown in Table 2.

Table 2

Grades from Fall 1984, Aero 371

	Student A	Student B	Student C	Course Average	Course Std Dev	Maximum Possible
Test #1	--	48	46	42.6	7.6	50
Test # 2	61	59	--	64.4	18.9	100
Test #3	86	--	70	57.7	15.4	100
Test #4	43	49	46	43.5	4.7	50
Test #5	66	60	52	72.1	14.5	100
AVG.	73. 14%	72.00%	71.33%	69.2%	12.2	

The same basic logic used in the earlier example can be used in this more complex one. Student A receives a 45 for Test #1 and now has an average of 75.25%. Student B receives a 57 for Test #3 and now has an average of 68.25%. Student C receives a 64 for Test #2 and now has an average of 69.50%. These imaginary grades corrected the

misplacement of these students in the order of merit which, in this case, has 76 students. Student A moved from 29 to 26, Student B moved from 34 to 43, and Student C moved from 36 to 41. Student A moved up because he missed an easy exam. Students B and C moved down because they missed hard exams, but Student C moved ahead of Student B.

Calculating the imaginary grades in this second example is more challenging than in the first example because not all exams were of equal weight. To handle problems like this and to enable automation of the procedure, I developed general methodology for the calculation of the imaginary grades.

III.   Methodical Calculation of Imaginary Grades

You can calculate the imaginary grades quite methodically by using the following equation:

$$x_{imag} = \bar{x}_{miss} + \frac{\sigma_{miss}}{\sum\limits_{n=1}^{N} x_{max,n}} \cdot \sum_{n=1}^{N} \left[\frac{x_{max,n} \cdot (x_n - \bar{x}_n)}{\sigma_n} \right]$$

where

x_{imag} = the imaginary score given on the missed exam

$\bar{x}_{miss}$ = the mean on the exam which was missed

σ_{miss} = the standard deviation on the exam which was missed

N = the total number of exams taken by the student in question

$x_{max,n}$ = the maximum number of points possible on Exam #n

x_n = the score achieved by the student in question on Exam #n

$\bar{x}_n$ = the mean on Exam #n

σ_n = the standard deviation on Exam #n

If you carefully study this equation, you can get some meaning from each term.

The term $(x_n - \bar{x}_n)$ is simply the difference between the student's score and the mean on Exam #n. By dividing this term by the standard deviation, you get the number of standard deviations away from the mean the student was on that test. Multiplying this number by the maximum score gives a number which is a weighted difference from the mean. By adding these weighted differences for each test that was taken, you arrive at the total difference from the mean for the whole course. That divided by the maximum possible points for the exams taken yields an average number of standard deviations from the mean for this student. Multiply that number by the standard deviation for the missed exam and add the result to the mean of the missed exam, and you arrive at the imaginary score for that exam.

A simplified form of the above equation results if all exams have the same maximum number of points available. The above equation reduces to

$$x_{imag} = \bar{x}_{miss} + \frac{\sigma_{miss}}{N} \cdot \sum_{n=1}^{N} ((x_n - \bar{x}_n)/\sigma_n)$$

This equation is easier to understand than the more general one. Note that it can be used on the first example in this paper, but not on the second example.

I wrote a computer program called FAKEGRD to assist in the implementation of the imaginary grade calculation. A listing of the program is attached as Appendix 1. This program reads the exam data from the course data disk, performs the calculation of the imaginary scores, and prints the results for each student who missed an exam. If the imaginary scores look reasonable, they should then be included on the course data disk.

IV. Cautions on the Use of FAKEGRD

I have a few recommendations and warnings concerning the calculation of

imaginary grades in general.

1. The imaginary grades should be determined after all graded work except the final has been entered to the course data disk. At the course director's discretion, Instructor Prerogative (IP) points and graded reports could also be used in the calculation of the imaginary scores. If the course director decides not to use all of the grades in the course file, he must create a new file and save it on the disk under a new name.

2. Do not give an imaginary score greater than 100% or less than 0%, regardless what the FAKEGRD program tells you. By calculating an imaginary score for a missed exam, we are trying to estimate what the student would have scored if hehadtaken the exam. He could not have scored greater than 100% if he had taken the exam.

3. Imaginary grades can and should be calculated at mid-term, but these grades should only be used qualitatively to help determine a mid-term letter grade. They should not be stored on the course grade disk at mid-term. A new imaginary grade will be calculated at the end of the semester after the student has established his position in the class standing.

V. Conclusion

Faculty workload will continue to be a problem. As we take steps to reduce it we must be careful to be as fair as possible to each student. The imaginary grade calculation described in this paper will ensure that, if a graded event is excused, a fair course grade will still be awarded.

APPENDIX 1

FAKEGRD

```
    1 $PAGESIZE: 61
    2 C
    3 C      ******************************************************************
    4 C      ******************************************************************
    5 C      ****************** PROGRAM FAKEGRD, 28 AUG 85  ******************
    6 C      ******************************************************************
    7 C      ******************************************************************
    8 C
    9        DIMENSION XB(14),X(14,200),MISS(14),XM(14),SD(14),AM(14),STUD(200)
   10        CHARACTER A*1,CRS*8,STUD*8,AM*1,EX*7,D*8,F*12,DAT*8
   11 C
   12 C      SET UP THE PROGRAM.
   13 C
   14        WRITE (*,1001)
   15 1001 FORMAT (//////////,' THIS PROGRAM IS FOR USE IN COURSES WITH LESS'
   16      1,' THAN 200 STUDENTS.',/,' IF YOUR COURSE HAS MORE THAN 200',
   17      2' STUDENTS, USE THE "CORE" VERSION OF FAKEGRD.',/,
   18      3' IF YOU WANT TO EXIT THIS',
   19      4' PROGRAM NOW, TYPE "STOP"; IF NOT, HIT "RETURN".',//////////)
   20        READ (*,2001) A
   21 2001 FORMAT (A1)
   22        IF (A.EQ.'S') STOP
   23        WRITE (*,1002)
   24 1002 FORMAT (//////,' THIS PROGRAM WILL PROVIDE YOU WITH IMAGINARY',
   25      1' SCORES FOR MISSED EXAMS.',//,' THE RESULTS WILL BE PRINTED, SO',
   26      2' TURN ON THE PRINTER.',//,' AFTER YOU GET THE RESULTS, CHECK',
   27      3' THEM CAREFULLY.',/,' IF THEY LOOK GOOD,',
   28      4' INPUT THEM MANUALLY USING THE "GRADER" PROGRAM.',/)
   29        WRITE (*,1003)
   30 1003 FORMAT (' NOTE:  IN DETERMINING THE IMAGINARY GRADES, YOU SHOULD',
   31      1' USE ALL',/,'          OF THE GRADES (EXCEPT THE FINAL) WHICH HAVE'
   32      2,' BEEN QUANTITATIVELY',/,'          ESTABLISHED.  IP POINTS MAY BE'
   33      3,' USED IF YOU WISH. ',/,'          IF YOU DO NOT WANT TO USE ALL',
   34      4' OF THE GRADES, CREATE A NEW',/,'          DATA FILE AND RENAME',
   35      5' IT.  IF YOU WANT TO LEAVE THE',/,'          PROGRAM NOW, TYPE',
   36      6' "STOP"; IF NOT, HIT "RETURN".'///////)
   37        READ (*,2001) A
   38        IF (A.EQ.'S') STOP
   39        WRITE (*,1004)
   40 1004 FORMAT (///,' TYPE YOUR COURSE WITH ".DAT" APPENDED (I.E. '
   41      1'"AERO356.DAT").',/,' NOTE:  IF YOU CREATED A NEW DATA FILE,'
   42      2' TYPE IN THAT NEW FILE NAME.',//////)
   43        READ (*,2002) F
   44 2002 FORMAT (A12)
   45        OPEN (5,FILE=F)
   46        OPEN (6,FILE='PRGRD',STATUS='NEW')
   47 C
   48 C      READ THE PRELIMINARY EXAM DATA FROM FILE "F".
   49 C
   50        WRITE (*,1005)
   51 1005 FORMAT (/,' NOW PLEASE INPUT THE NUMBER OF STUDENTS IN YOUR',
   52      1' COURSE AND THE NUMBER OF EXAMS GIVEN.',////,
   53      2' THE NUMBERS SHOWN BELOW ARE THE NUMBERS YOU SHOULD TYPE IN.',/)
   54        READ (5,2003) CRS,DAT
```

```
      55  2003 FORMAT (A8,/,8X,A8)
      56    93 WRITE (*,1006) DAT
      57  1006 FORMAT (1X,A8,//' TYPE IN THE FIRST NUMBER, THE NUMBER OF',
      58       1' STUDENTS, AND HIT RETURN.')
      59       READ (*,2004) NSTUDS
      60  2004 FORMAT (I4)
      61       WRITE (*,1007)
      62  1007 FORMAT (' NOW TYPE IN THE SECOND NUMBER, THE NUMBER OF',
      63       1' EXAMS, AND HIT RETURN.')
      64       READ (*,2004) NEXAMS
      65       WRITE (*,1008) NSTUDS,NEXAMS
      66  1008 FORMAT (///,' DO THESE NUMBERS,',I4,' AND',I3,', MATCH THE',
      67       1' ONES I PRINTED?')
      68       READ (*,2001) A
      69       IF (A.EQ.'Y') GO TO 95
      70       GO TO 93
      71    95 IF (NEXAMS.LT.9) GO TO 100
      72       WRITE (*,1009)
      73  1009 FORMAT (//,' YOU SHOULD HAVE TYPED "COMPRESS" BEFORE "FAKEGRD".'
      74       1,/,'    IF YOU DID NOT, TYPE "STOP", THEN "COMPRESS", THEN ',
      75       2'"FAKEGRD".',/,'    IF YOU DID, JUST HIT "RETURN".')
      76       READ (*,2001) A
      77       IF (A.EQ.'S') STOP
      78 C
      79 C     READ IN ALL OF THE EXAM SCORES FOR EACH STUDENT.
      80 C
      81   100 WRITE (*,1010)
      82  1010 FORMAT (//////////,' THE CALCULATIONS ARE UNDERWAY.',//,
      83       1' SIT BACK AND RELAX; THIS MAY TAKE A WHILE.',////////////)
      84       READ (5,2005) (XM(I),I=1,NEXAMS)
      85  2005 FORMAT (/,20(F3.0,1X))
      86       TOT = 0.
      87       DO 150 I=1,NEXAMS
1     88   150 TOT=TOT+XM(I)
      89       DO 200 N=1,NSTUDS
1     90   200 READ (5,2006) STUD(N),(X(I,N),I=1,NEXAMS)
      91  2006 FORMAT (A8,21X,20F4.0)
      92       EX='  EXAM#'
      93       D='--------'
      94 C
      95 C     CALCULATE THE MEANS AND STANDARD DEVIATIONS
      96 C
      97       DO 300 I=1,NEXAMS
1     98       STUDS = 0.
1     99       XB(I) = 0.
1    100           DO 250 N=1,NSTUDS
2    101           IF (X(I,N).LT.0.) GO TO 250
2    102           STUDS = STUDS + 1.
2    103           XB(I) = XB(I) + X(I,N)
2    104   250     CONTINUE
1    105   300 XB(I) = XB(I)/STUDS
     106       DO 400 I=1,NEXAMS
1    107       STUDS = 0.
1    108       SD(I) = 0.
```

77

```
D Line# 1     7
1   109              DO 350 N=1,NSTUDS
2   110              IF (X(I,N).LT.0.) GO TO 350
2   111              STUDS = STUDS + 1.
2   112              SD(I) = SD(I) + (X(I,N) - XB(I))**2
2   113     350      CONTINUE
1   114     400  SD(I) = SQRT(SD(I)/(STUDS - 1.))
    115 C
    116 C      SEND THE HEADING TO THE PRINT FILE
    117 C
    118          WRITE (6,1011) CRS
    119   1011 FORMAT (////,30X,'FAKE GRADES FOR ',A8,//)
    120          WRITE (6,1012)
    121   1012 FORMAT (' NOTE:  ASTERISKS (*) IDENTIFY THE IMAGINARY',
    122        1' SCORES.',/)
    123          WRITE (6,1013) (EX,I,I=1,NEXAMS)
    124   1013 FORMAT (/,' STUDENT  NEW AVG',15(A7,I1))
    125          WRITE (6,1014) (D,I=1,NEXAMS)
    126   1014 FORMAT (' ----------------',15A8)
    127 C
    128 C      EVALUATE THE SUMMATIONS NECESSARY FOR THE CALCULATION.
    129 C
    130          DO 500 N=1,NSTUDS
1   131          TERM=0
1   132          XMAX=0
1   133          NOMISS=0
1   134          K=1
1   135              DO 420 I=1,NEXAMS
2   136              AM(I)=' '
2   137              IF (X(I,N).GE.0.) GO TO 410
2   138              MISS(K)=I
2   139              NOMISS=1
2   140              K=K+1
2   141              GO TO 420
2   142     410      XMAX=XMAX+XM(I)
2   143              TERM=TERM+XM(I)*(X(I,N)-XB(I))/SD(I)
2   144     420      CONTINUE
1   145          IF (NOMISS.EQ.0) GO TO 500
1   146          K=K-1
1   147 C
1   148 C      CALCULATE THE IMAGINARY GRADE(S).
1   149 C
1   150              DO 440 I=1,K
2   151              M=MISS(I)
2   152              X(M,N)=XB(M)+SD(M)*TERM/XMAX
2   153              AM(M)='*'
2   154     440      CONTINUE
1   155 C
1   156 C      SEND THE CALCULATED INFORMATION TO THE PRINT FILE.
1   157 C
1   158          AVG=0.
1   159              DO 450 I=1,NEXAMS
2   160     450      AVG=AVG+X(I,N)
1   161          AVG=100.*AVG/TOT
1   162          WRITE (6,1015) STUD(N),AVG,(X(I,N),AM(I),I=1,NEXAMS)
```

D Line# 1   7   Microsoft FORTRAN77 V3.10 05/03/83

```
 1   163  1015  FORMAT (1X,A8,F7.2,10(F7.0,A1))
 1   164   500  CONTINUE
     165         WRITE (6,1014) (D,I=1,NEXAMS)
     166         WRITE (6,1016) (XM(I),I=1,NEXAMS)
     167  1016  FORMAT (' MAX',13X,14F8.1)
     168         WRITE (6,1017) (XB(I),I=1,NEXAMS)
     169  1017  FORMAT (' MEAN',12X,14F8.2)
     170         WRITE (6,1018) (SD(I),I=1,NEXAMS)
     171  1018  FORMAT (' STD DEV',9X,14F8.2)
     172         WRITE (6,1019)
     173  1019  FORMAT (//,' ENSURE ACCURACY BY:',/,
     174        1'     1.  LOOKING FOR "WAY-OUT" NUMBERS LIKE ZERO.',/,
     175        2'     2.  CHECKING THE FAKE GRADES FOR REASONABLENESS.',/,
     176        3'     3.  ENSURING THAT THERE IS A FAKE GRADE FOR EVERY'
     177        4' MISSING GRADE.',/,
     178        5'     4.  COMPARING THE MEAN AND STD DEV HERE AGAINST A',
     179        6' "GRADER" OUTPUT.',//)
     180         WRITE (6,1020)
     181  1020  FORMAT(/,' NOTE:  DO NOT INPUT FAKE GRADES',
     182        1' TO THE "GRADER" PROGRAM AT THE PROG.',/,7X,
     183        2' JUST USE THIS INFORMATION TO HELP YOU ASSIGN PROG GRADES.',/
     184        3,7X,' INPUT THE FAKE GRADES USING "GRADER" AT THE END OF THE',
     185        4' SEMESTER ONLY.')
     186         CLOSE (5)
     187         CLOSE (6)
     188         WRITE (*,1021)
     189  1021  FORMAT (/,' I AM SENDING THE RESULTS TO THE PRINTER NOW.',
     190        1///,' IT HAS BEEN A PLEASURE WORKING WITH YOU.',/////////)
     191         STOP
     192         END
```

Name	Type	Offset	P Class
A	CHAR*1	13360	
AM	CHAR*1	13026	
AVG	REAL	15418	
CRS	CHAR*8	14486	
D	CHAR*8	15151	
DAT	CHAR*8	14494	
EX	CHAR*7	15144	
F	CHAR*12	14274	
I	INTEGER*4	15088	
K	INTEGER*4	15402	
M	INTEGER*4	15414	
MISS	INTEGER*4	11314	
N	INTEGER*4	15120	
NEXAMS	INTEGER*4	14704	
NOMISS	INTEGER*4	15398	
NSTUDS	INTEGER*4	14606	
SD	REAL	11370	
SQRT			INTRINSIC
STUD	CHAR*8	11426	
STUDS	REAL	15164	
TERM	REAL	15390	

D Line# 1   7

TOT	REAL	15112
X	REAL	114
XB	REAL	2
XM	REAL	58
XMAX	REAL	15394

Name	Type	Size	Class
MAIN			PROGRAM

Pass One   No Errors Detected
             192 Source Lines

END

FILMED

3 -86

DTIC